

RI 9569

**RI 9569**

**REPORT OF INVESTIGATIONS/1995**

PLEASE DO NOT REMOVE FROM LIBRARY



LIBRARY  
SPOKANE RESEARCH CENTER  
RECEIVED

NOV 1 1995

US BUREAU OF MINES  
E. 315 MONTGOMERY AVE.  
SPOKANE, WA 99207

# Leaching Pyrite From Coal Waste: Results of Diagnostic Study

UNITED STATES DEPARTMENT OF THE INTERIOR



UNITED STATES BUREAU OF MINES

**Report of Investigations 9569**

**Leaching Pyrite From Coal Waste:  
Results of Diagnostic Study**

**By Robert F. Chaiken and Louis E. Dalverny**

**UNITED STATES DEPARTMENT OF THE INTERIOR  
Bruce Babbitt, Secretary**

**BUREAU OF MINES  
Rhea Lydia Graham, Director**

International Standard Serial Number  
ISSN 1066-5552

## CONTENTS

	<i>Page</i>
Abstract .....	1
Introduction .....	2
Theoretical basis .....	2
Application to pyrite leaching from coal and coal waste .....	4
Data of experiment 1 .....	7
Data of experiment 2 .....	12
Data of experiment 3 .....	14
Data of experiment 4 .....	14
Kinetic interpretations .....	28
Rates of reaction and stoichiometry .....	28
Reaction order .....	31
Mechanisms .....	34
Descriptive considerations .....	34
Model considerations .....	35
Accelerated leaching of pyrite .....	37
Conclusions .....	38
Acknowledgments .....	38
References .....	39
Appendix A.—A/D model of solids leaching .....	40
Appendix B.—List of symbols .....	42

## ILLUSTRATIONS

1. Schematic of counterflow, trickle-bed, packed-column reactor .....	4
2. Experiment 1: O <sub>2</sub> consumption within column .....	8
3. Gas and liquid flow rates for experiments 1 to 4 .....	9
4. Experiment 1: SO <sub>4</sub> <sup>2-</sup> concentration in lixiviant solution at station 7 .....	11
5. Experiment 1: Fe <sup>3+</sup> and H <sup>+</sup> concentration in lixiviant solution at station 7 .....	11
6. Experiments 1 to 4: correlation of THC with O <sub>2</sub> consumption .....	12
7. Experiment 1: CO <sub>2</sub> gas production within column .....	13
8. Experiment 1: most probable number of bacteria measurement for lixiviant solution at station 7 .....	14
9. Experiment 2: SO <sub>4</sub> <sup>2-</sup> concentration in lixiviant solution .....	15
10. Experiment 2: O <sub>2</sub> consumption within column .....	16
11. Experiment 2: ion concentrations in lixiviant solution at station 7 .....	17
12. Experiment 2: THC within column .....	18
13. Experiment 2: CO <sub>2</sub> gas concentration within column .....	19
14. Experiment 2: most probable number of bacteria measurement for lixiviant solution within column ..	20
15. Experiment 3: total O <sub>2</sub> consumption and O <sub>2</sub> consumption for other than CO <sub>2</sub> at station 0 .....	20
16. Experiment 3: SO <sub>4</sub> <sup>2-</sup> concentration in lixiviant solution .....	21
17. Experiment 3: THC within column .....	22
18. Experiment 3: H <sup>+</sup> concentration in lixiviant solution .....	23
19. Experiment 3: Fe <sup>3+</sup> concentration in lixiviant solution at station 7 .....	24
20. Experiment 3: CO <sub>2</sub> gas concentration at station 0 .....	24
21. Experiment 4: O <sub>2</sub> consumption and gas flow rate at station 0 .....	25
22. Experiment 4: gas concentrations within column .....	26
23. Experiment 4: ion concentrations in lixiviant solution at station 7 .....	27
24. Experiments 1 to 4: rates of production of ions and consumption of O <sub>2</sub> within column .....	28
25. Experiments 1 to 4: stoichiometries for O <sub>2</sub> , Fe <sup>3+</sup> , and H <sup>+</sup> relative to SO <sub>4</sub> <sup>2-</sup> .....	29
26. Experiments 1 to 4: rate of reaction of pyrite within column .....	31
27. Experiments 1 to 4: extent of pyrite removal within column .....	32

## ILLUSTRATIONS—Continued

	<i>Page</i>
28. Experiments 1 to 4: test of reaction orders from kinetic data and concentrations .....	33
29. Comparison of A/D model rate of pyrite reaction calculations with experiment .....	36
A-1. Examples of shortest distances in particle .....	40
A-2. Representation of diffusion process in A/D model .....	41

## TABLES

1. Experiment 1: results of solids analyses .....	5
2. Experiment 2: results of solids analyses .....	5
3. Experiment 3: results of solids analyses .....	6
4. Experiment 4: results of solids analyses .....	6
5. Experiments 1 to 4: experimental curve-fit parameters .....	10
6. Averaged stoichiometric ratios .....	29
7. Experiments 1 to 4: A/D model curve-fit parameters .....	37

## UNIT OF MEASURE ABBREVIATIONS USED IN THIS REPORT

cm	centimeter	mL/min	milliliter per minute
cm/d	centimeter per day	(mmol/d)/L	millimole per day per liter
cm <sup>2</sup> /s	square centimeter per second	mmol/L	millimole per liter
ft	foot	mol	mole
kg	kilogram	pct	percent
kJ/kg	kilojoule per kilogram	ppm	part per million
L/d	liter per day	μm	micrometer
m	meter	μmol	micromole
m/d	meter per day	(μmol/d)/L	micromole per day per liter
mg/L	milligram per liter		

# LEACHING PYRITE FROM COAL WASTE: RESULTS OF DIAGNOSTIC STUDY

By Robert F. Chaiken<sup>1</sup> and Louis E. Dalverny<sup>2</sup>

---

## ABSTRACT

The U.S. Bureau of Mines conducted an experimental and theoretical study of coupled chemical kinetic and mass transport processes during leaching of pyrite from coal in a counterflow, "trickle-bed" column reactor. Spatial and temporal data on reactant and product concentrations were used as solutions to appropriate continuity equations, which in turn define chemical kinetic reaction rates. Data from four 180- by 30-cm column leaching experiments using coal, coal waste, and air-water and air-FeCl<sub>3</sub> lixiviants have been analyzed. The rate of leaching was found to be diffusion limited (probably by Fe<sup>3+</sup>) and not controlled by bacterial action. Rates of pyrite oxidation were found to vary with elapsed time (80 to 225 days) and followed a bell-shaped curve, sometimes with a delay before start of reaction. Maximum rates of reaction ranged from 3 to 10 (mmol/d)/L (column) for coal waste and 0.4 (mmol/d)/L (column) for coal. Reaction was 30 to 80 pct complete, probably due to precipitation of product salts (e.g., jarosites), which impede transport of oxidant through the coal.

An absorption-desorption model of solids leaching, which considers the role of heterogeneous porosity in solids leaching, was used to describe time-dependent leaching rates.

---

<sup>1</sup>Research chemist.

<sup>2</sup>Physicist.

Pittsburgh Research Center, U.S. Bureau of Mines, Pittsburgh, PA.

## INTRODUCTION

Leaching of solids is of considerable interest to the U.S. Bureau of Mines (USBM) and the minerals industry from a number of aspects (1).<sup>3</sup> Leaching has potential use for (1) the recovery of metals from low-grade ores (2), (2) the removal of pyrite from coal and coal waste (3),<sup>4</sup> (3) the recovery of fuels from coal wastes, (4) the evaluation of groundwater contamination from mine wastes (4), and (5) the removal of solutes onto solid substrates (5).<sup>5</sup> The leaching process involves a coupling of chemical reactions and transport phenomena in a multicomponent, multiphase reaction system. The coupled process can be analyzed by directly measuring the coupled reaction-transport conditions in model and actual leach systems.

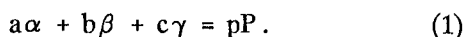
This approach differs from many previous studies of solid leach processes in which reaction kinetics and transport were studied in an uncoupled mode (2, 6). For example, reaction rates were measured under isothermal stirred conditions and flows were measured in nonreacting fluids. These reaction and transport data are then coupled through mathematical treatment of the process. Comparing the results of such mathematical treatments with actual leach data is often little more than curve fitting. Although it can lead to a correlation of the data, it can often miss

describing the mechanism(s) that actually control the leach process. Yet, it is only through an understanding of these actual mechanisms that solid leaching processes can be effectively predicted and optimized.

This Report of Investigations presents a mathematical description of a multiphase system of reactive gaseous and liquid components moving one dimensionally through a column of particulate solids (i.e., a fixed-bed column reactor). The resulting equations are then applied to actual pyrite leaching data obtained with a counterflow, trickle-bed column reactor (0.3-m diameter, 1.8-m length) (7) to elucidate the operating mechanisms that control the leach process. The interpretive analyses described in this report are believed to represent a significant methodology for determining reaction mechanisms and an approach that can be generalized and applied to the study of numerous other solids leaching systems. As a direct result of this methodology, a new model for transport limited chemical reaction in solids was developed at the USBM where the heterogeneity of the particles (e.g., size, shape, porosity, etc.) can be accounted for, in principle, directly through the use of distribution theory (8).

## THEORETICAL BASIS

Consider a multiphase system of reacting gaseous, liquid, and solid components distributed along a column. The reaction within the column can be described as



Here,  $\alpha$ ,  $\beta$ , and  $\gamma$  represent the gaseous, liquid, and solid-phase reactants and  $a$ ,  $b$ , and  $c$  their respective reaction stoichiometries to produce  $p$  moles of product,  $P$ .<sup>6</sup> Taking the system geometry as one dimensional, a generalized rate of reaction at any point and time ( $R_p$ ) can be written as

$$R_p = k_r \alpha^{a'} \beta^{b'} \gamma^{c'} = F(\alpha, \beta, \gamma) = G(x, t), \quad (2)$$

$$\text{leading to } P = f(\alpha, \beta, \gamma, t) = g(x, t). \quad (3)$$

Here,  $\alpha$ ,  $\beta$ ,  $\gamma$ , and  $P$  now represent the concentration of reactants and products (e.g., mol/cm<sup>3</sup> of column volume),  $a'$ ,  $b'$ , and  $c'$  are their respective reaction orders, which are not necessarily the same as the stoichiometric coefficients, and  $k_r$  is the rate constant for the overall reaction. The  $f$  and  $g$  functions (lower and upper case) represent two different coordinate systems that can be used to express the kinetic reaction rate and the product concentration. The  $g$  functions arise from the time ( $t$ ) and space ( $x$ ) dependency of the reactant concentrations within the column, i.e.,

$$\alpha = \phi(x, t),$$

$$\beta = \psi(x, t),$$

and

$$\gamma = \theta(x, t). \quad (4)$$

<sup>3</sup>Italic numbers in parentheses refer to items in the list of references preceding the appendixes at the end of this report.

<sup>4</sup>Removal of Pyrite From Coal by Heap Leaching by L. M. Cathles and K. J. Breen. Final report on USBM grants G5105007, G5115007, and G1115427, June 1983, 263 pp.

<sup>5</sup>Absorption of metals and other ionic species from solution onto solid substrates may be considered the converse to the leaching of solids.

<sup>6</sup>Each phase can be composed of a sum of reactant species and products that can be distinguished by numerically subscripting  $\alpha$ ,  $\beta$ ,  $\gamma$ ,  $P$ ,  $a$ ,  $b$ ,  $c$ , and  $p$ . For the sake of clarity, these subscripts, the specific reaction rates, and applicable continuity equations are not written explicitly, but simply implied.

For gas ( $\phi$ ) and liquid ( $\psi$ ) phases that move through the column and a solid ( $\theta$ ) phase that remains stationary (i.e., a fixed-bed reactor), the following equations will apply (9):

$$\epsilon(1 - s)(\phi)_t = -(\phi v_\alpha)_x + R_\alpha,$$

$$\epsilon s(\psi)_t = -(\psi v_\beta)_x + R_\beta,$$

and  $(1 - \epsilon)(\theta)_t = R_\gamma,$  (5)

where  $\epsilon$  = porosity (i.e., void volume fraction),

$s$  = saturation (i.e., fraction of void volume that is filled with liquid),

$\phi$  =  $\phi(x,t)$ , concentration of component of  $\alpha$ , expressed as quantity (mass or moles) per unit volume of  $\alpha$ , i.e., generally, value as measured,

$\psi$  =  $\psi(x,t)$ , concentration of component of  $\beta$ , expressed as quantity (mass or moles) per unit volume of  $\beta$ , i.e., generally, value as measured,

$\theta$  =  $\theta(x,t)$ , concentration of component of  $\gamma$ , expressed as quantity (mass or moles) per unit volume of  $\gamma$ , i.e., generally, value as measured,

$v_{\alpha,\beta}$  = effective linear velocity of gas and liquid flows, i.e., value of measured volumetric fluid flow rate divided by column cross section,

and  $R_{\alpha,\beta,\gamma}$  = kinetic terms describing rate of production (or disappearance) of gas, liquid, and solid components expressed as quantity (mass or moles) per unit of *column* volume per unit of time, i.e., generally, *not* value as measured.

In the above equations, the distinction between concentrations as normalized to phase volume (i.e., gas, liquid, or solid) and as normalized to reaction (or column) volume must be recognized. Also, it is assumed that convective

transport is dominating the flow of fluids along the column. That is, diffusive flow in the axial direction is neglected. This latter assumption can be lifted by adding a second-order diffusion term to the right-hand side (RHS) of equation 5 (9). Axial diffusive flow would not negate the diagnostic methodology to be described, but would complicate it somewhat.

The functions  $\phi(x,t)$ ,  $\psi(x,t)$ , and  $\theta(x,t)$  actually represent solutions to the above partial differential equations so that if these functions were determined experimentally, the equations would yield the individual kinetic rates,  $R_{\alpha,\beta,\gamma}$ . This is the key to the diagnostic methodology as proposed for the design and execution of experiments with column bed reactors. Sufficient experimental data are taken to define concentrations as a function of time and space. Curve-fitting techniques are then applied to the experimental data to yield analytic expressions for the concentration functions (in time and space), which can then become the basis for determining the appropriate kinetic rates of consumption of reactants and production of products. Since the concentrations are determined during actual leaching conditions where the reaction and transport processes are coupled, the reaction rates as determined will likewise be those that occur under actual coupled conditions. Hence, at a minimum, they should be valid over the range of operating conditions encountered during the experiment. With mechanistic insights afforded by data interpretations, the rates should also be extrapolatable to other operating conditions.

For example, reaction stoichiometries during the leaching process can be obtained from the ratio of the values of  $R_{\alpha,\beta,\gamma}$ , as determined from equation 5. The reaction orders  $a'$ ,  $b'$ , and  $c'$  (or at least constraints on their values) can be obtained from differential forms of equation 2, e.g.,

$$\frac{d \ln R_p}{d \ln \alpha} = a' + b' \frac{d \ln \beta}{d \ln \alpha} + c' \frac{d \ln \gamma}{d \ln \alpha}. \quad (6)$$

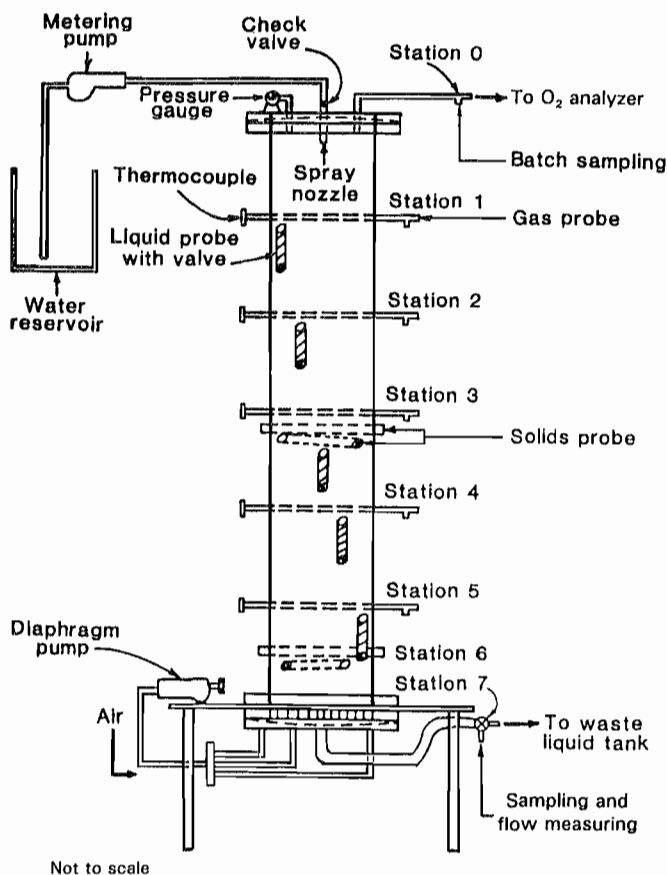
A special case of interest would be the achievement of a maximum rate within the column bed reactor, i.e., where  $dR_p/dx = 0$ . This would not only yield an additional constraint on the reaction orders, but would also indicate optimum operating conditions for accelerating the leaching (e.g., pyrite from coal waste). As described in the "Reaction Order" section, this constraint was apparently not achieved with the size of reactor and conditions of flow used in the study reported here.

## APPLICATION TO PYRITE LEACHING FROM COAL AND COAL WASTE

Experimental aspects of the trickle-bed column reactor and its operations are described in the experimental report (7).<sup>7</sup> Briefly, the reactor consisted of a heavy wall acrylic tube (180-cm long, 30-cm diameter) with gas, liquid, and solid sampling probes positioned through the tube wall approximately every 30 cm along the reactor (figure 1). The packed bed consisted of particles of coal waste (cleaning plant reject material) or of cleaned coal having a size ranging from 2 to 4 cm. Lixiviant (filtered tap water or  $\text{FeCl}_3$  solution) was metered onto the top of the bed while gas (air) was metered into the bottom of the bed to create a counterflow arrangement of downward-moving lixiviant with leachate concentration increasing with flow distance and an upward-flowing gas stream with  $\text{O}_2$  concentration decreasing with flow distance. The local concentration of

<sup>7</sup>Reference 7 contains a preliminary description of the first two column leaching experiments. A complete report of the column studies is currently in progress.

**Figure 1**



**Schematic of counterflow, trickle-bed, packed-column reactor.**

reactants and products, and possibly the reaction rate, varied continuously along the length of the reactor. Inlet flow rates of liquid and air were kept constant during an experiment, but that did not always lead to constant outflows. This affected some of the data analyses, as will be discussed later on in connection with the specific column experiment. Liquid and gas samples were taken several times each day, whereas solids were sampled only once or twice during leaching. Chemical analyses involved conventional methods of wet chemistry for the liquids, chromatography for the gases, and standard coal analyses for the solids.

Four experiments were carried out with several objectives in mind and with varying degrees of success in their operation.

Experiment 1 involved approximately 145 kg of nearly fresh coal waste obtained from a nearby coal cleaning plant. The ultimate analysis for this material indicated a pyritic sulfur content of 5.37 pct (table 1). Over the 160 days of this experiment, difficulties were encountered in obtaining liquid samples on a daily basis and in maintaining constant flows, but the gas data and some liquid data that were obtained were significant in terms of their relationship to the leaching process. The process exhibited an apparent 35-day lag to produce a measurable leaching rate, which then peaked at about day 70 (elapsed time).

Experiment 2 was essentially a repeat of the first experiment with the intent of resolving the previously encountered liquid sampling and fluid control problems. The coal waste in experiment 2, while coming from the same lot as that used earlier, was apparently partially leached to start with, having been stored outside under a tarpaulin with only limited protection against the weather. This can be surmised directly from the ultimate analysis (table 2), which indicates more sulfate sulfur and less pyritic sulfur in the coal waste than was found for the coal waste used in experiment 1. The weathered sample did not exhibit a lag time before leaching, and its reaction peak occurred at about elapsed day 35. The sampling of gases and liquids were improved in experiment 2, and the data proved amenable to curve-fitting and reaction rate analysis.

Experiment 3 involved an 85-kg sample of cleaned coal (Pittsburgh No. 8), which was particularly low in carbonate content and whose pyrite was finely disseminated (table 3). This coal was used to examine the effect of acid-buffering capacity on the pyrite leach process since the coal waste was particularly high in carbonate (reported as  $\text{CO}_2$  in tables 1 through 4). This coal was also the object of studies involving bioleaching as a coal beneficiation process (10-11).

Table 1.—Experiment 1: results of solids analyses<sup>1,2</sup>

Elapsed time, days	Sample	Analysis, pct					Heat value, kJ/kg	pct of original S normalized to ash			Excess S, pct						
		H	C	N	O	Ash		Sulfate S	Pyritic S	Organic S	CO <sub>2</sub>	Sulfate	Pyritic	Organic	Sulfate	Organic	Total
0	Original	1.57	19.78	0.28	3.64	69.29	0.06	5.37	0.01	0.56	11,730	100	100	100	0	0	0
77	Station 3	1.74	18.90	0.30	5.84	70.75	0.67	1.66	0.14	0.08	11,720	1,094	30	1,371	61	13	74
77	Station 6	1.58	15.81	0.26	5.70	73.84	0.72	1.97	0.12	0.16	9,220	1,126	34	1,126	66	11	77
160	Top	1.62	18.22	0.44	3.95	73.42	0.31	1.97	0.07	0.59	9,620	488	35	661	25	6	31
160	Bottom	1.66	16.81	0.44	4.23	74.68	0.12	1.93	0.13	0.19	9,460	186	33	1,206	6	12	18

<sup>1</sup>Ultimate analysis of materials (dry).<sup>2</sup>Column loading = 145 kg coal waste.Table 2.—Experiment 2: results of solids analyses<sup>1,2</sup>

Elapsed time, days	Sample	Analysis, pct					Heat value, kJ/kg	pct of original S normalized to ash			Excess S, pct						
		H	C	N	O	Ash		Sulfate S	Pyritic S	Organic S	CO <sub>2</sub>	Sulfate	Pyritic	Organic	Sulfate	Organic	Total
0	Original	1.62	18.39	0.35	4.79	69.33	1.16	3.71	0.05	0.34	10,750	100	100	100	0	0	0
125	Station 3	1.74	18.90	0.30	5.84	70.75	0.67	1.66	0.14	0.08	11,720	57	44	274	0	9	9
125	Station 6	1.58	15.81	0.26	5.70	73.84	0.72	1.97	0.12	0.16	9,220	58	50	225	0	7	7
216	Station 3	1.70	19.03	0.32	5.80	70.98	0.64	1.40	0.13	0.11	10,690	54	37	254	0	8	8
216	Station 6	1.59	18.60	0.32	5.44	71.17	0.67	2.00	0.21	0.10	10,690	56	53	409	0	16	16
277	End	1.68	19.55	0.38	5.59	70.31	0.57	1.75	0.17	0.30	11,200	48	47	328	0	12	12

<sup>1</sup>Ultimate analysis of materials (dry).<sup>2</sup>Column loading = 138 kg coal waste.

Table 3.—Experiment 3: results of solids analyses<sup>1,2</sup>

Elapsed time, days	Sample	Analysis, pct					Heat value, kJ/kg	pct of original S normalized to ash			Excess S, pct						
		H	C	N	O	Ash		Sulfate S	Pyritic S	Organic S	CO <sub>2</sub>	Sulfate	Pyritic	Organic	Sulfate	Organic	Total
0	Combination ..	5.23	73.46	1.23	6.71	9.11	0.01	1.99	2.26	0.24	45,670	100	100	100	0	0	
204	Combination ..	5.28	74.15	1.29	5.90	9.17	0.12	1.67	2.42	0.06	456,303	1,192	83	106	11	16	27

<sup>1</sup>Ultimate analysis of materials (dry).<sup>2</sup>Column loading = 85.5 kg coal.Table 4.—Experiment 4: results of solids analyses<sup>1,2</sup>

Elapsed time, days	Sample	Analysis, pct					Heat value, kJ/kg	pct of original S normalized to ash			Excess S, pct					
		H	C	N	O	Ash		Sulfate S	Pyritic S	Organic S	CO <sub>2</sub>	Sulfate	Pyritic	Organic	Sulfate	Organic
0	Original .....	1.51	16.11	0.32	2.55	73.83	0.04	5.55	0.09	0.60	10,050	100	100	100	0	0
80	Station 2 .....	1.33	15.99	0.23	3.45	73.98	0.02	3.70	1.30	0.28	9,580	50	67	1,442	0	121
80	Station 6 .....	1.36	15.66	0.25	4.26	73.20	0.03	3.57	1.67	0.30	9,100	76	65	1,872	0	158

<sup>1</sup>Ultimate analysis of materials (dry).<sup>2</sup>Column loading = 153 kg coal waste.

A fourth experiment was attempted with coal waste freshly obtained from the same source as for experiment 1 (table 4), but this time the initial lixiviant was a 500-ppm (on average) solution of  $\text{Fe}^{3+}$  as  $\text{FeCl}_3$ . The primary objective of this experiment was to see if  $\text{Fe}^{3+}$  would serve to accelerate the pyrite oxidation, since  $\text{Fe}^{3+}$  will oxidize pyrite (12-13), i.e.,



A secondary intended effect of the use of  $\text{FeCl}_3$  solution as a lixiviant was the possible inhibition of bacteria growth, thereby minimizing the effect of bacteria on the leaching process. For example, *Thiobacillus ferrooxidans* in a sulfuric acid solution can greatly accelerate the reaction



which occurs during leaching of pyrite from coal (13).

In each experiment, diagnostic sampling was carried out (or attempted) daily through liquid and gas probes placed about 30 cm apart along the 1.8-m column. Gas samples were analyzed for  $\text{O}_2$ ,  $\text{CO}_2$ , CO, and C1 to C5 hydrocarbons (THC). Liquid samples were analyzed for  $\text{SO}_4^{2-}$ ,  $\text{H}^+$ ,  $\text{Fe}^{2+}$ ,  $\text{Fe}^{3+}$ , and other metal ions. Only a few solid samples were obtained during each experiment, and they were submitted for ultimate analyses (tables 1 through 4).

## DATA OF EXPERIMENT 1

Figure 2 depicts the  $\text{O}_2$  consumption observed at the five stations that were available. Station 0 refers to the space just above the top of the coal waste where gases exited the bed since air was being introduced at the bottom and flowed upward. Station 7 is the efflux from the bottom of the bed since water was being introduced at the top to flow downward (see figure 1).

In spite of the data scatter, it is apparent that the consumed  $\text{O}_2$  over the 160-day duration of the experiment follows a somewhat skewed bell-type curve centered at about day 80, with an apparent 30- to 40-day lag to the onset of observable  $\text{O}_2$  consumption. This time delay to measurable reaction is much greater than the 4-day liquid and 0.25-day gas transit time through the column. Figure 3, which shows the measured flow rates for all four experiments, depicts the difficulties that were experienced in maintaining the constant for both gas and liquid flows during experiment 1.

The change in  $\text{O}_2$  consumption with distance in the column was observed to be approximately constant. This factor, combined with the bell-type distribution, led to the curve-fitted  $\phi(x,t)$  expression for  $\text{O}_2$  consumption shown in table 5 and plotted in figure 2. As figure 2 indicates, this curve-fit expression is a reasonable representation of the experiment 1  $\text{O}_2$  data at all the sampling stations. As

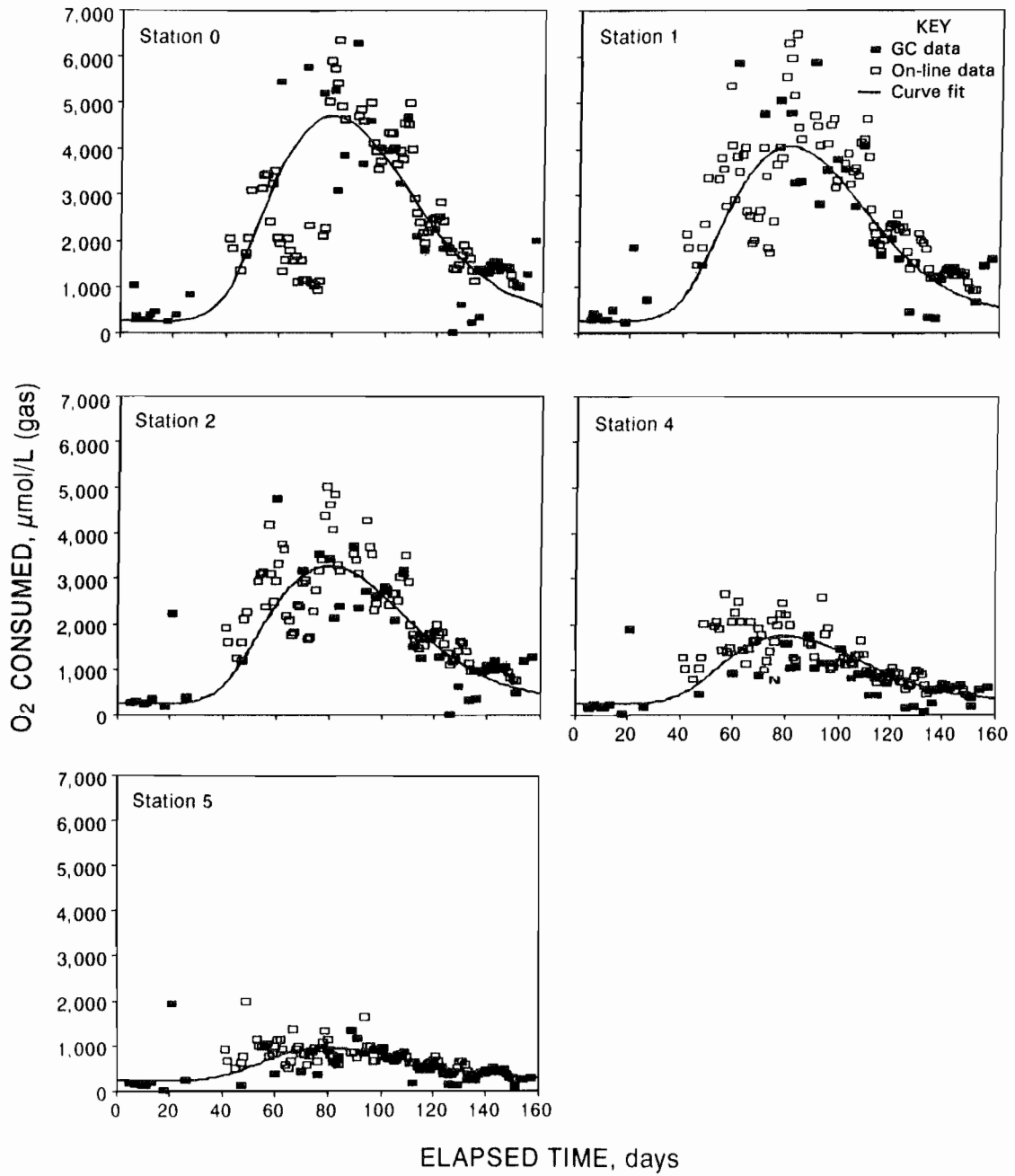
table 5 indicates and as discussed in the "Kinetic Interpretations" section, this form of equation worked well for curve fitting most of the leach data from all the experiments and served as the basis for developing an absorption-desorption (A/D) model for solids leaching (8). This new model will also be discussed in the "Mechanisms" section.

The only sampling station that yielded adequate liquid samples for chemical analysis was station 7 (i.e., the bottom efflux). Figure 4 depicts the measured  $\text{SO}_4^{2-}$  in solution at that station. Curve fitting in both  $x$  and  $t$  was not considered feasible because of the amount of scatter shown by this data; however, it is probable that the sulfate production followed the  $\text{O}_2$  consumption curve. Comparing the  $\text{SO}_4^{2-}$  concentration at station 7 with the  $\text{O}_2$  consumption at station 0 suggests a 30- to 40-day delay to reaction and a peak at about day 80. The curve labeled "curve fit" shown in figure 4 is actually the  $\text{O}_2$  consumption equation normalized to the range of the sulfate concentrations. Figure 5 depicts the measured  $\text{H}^+$  and FeD concentrations at station 7. While fewer in number, they are likewise consistent with the shape of the  $\text{O}_2$  consumption curve, which as in the case of the sulfate is the basis of the curve fits as shown. As long as air was flowing through the column, little if any  $\text{Fe}^{2+}$  was observed in solution.

An observation of interest from experiment 1 is the apparent linear relationship between consumption of  $\text{O}_2$  and production of THC (total C1 to C5 hydrocarbon gases consisting of the alkanes methane, ethane, propane, butane, and pentane). This is shown in figure 6, which depicts the plot of  $\text{O}_2$  consumption versus THC for all four experiments. These data will be discussed in detail in the "Kinetic Interpretations" section, but it should be noted that THC are not oxidation products of coal, but known degasification products, e.g., as in the desorption of methane from coal (14).

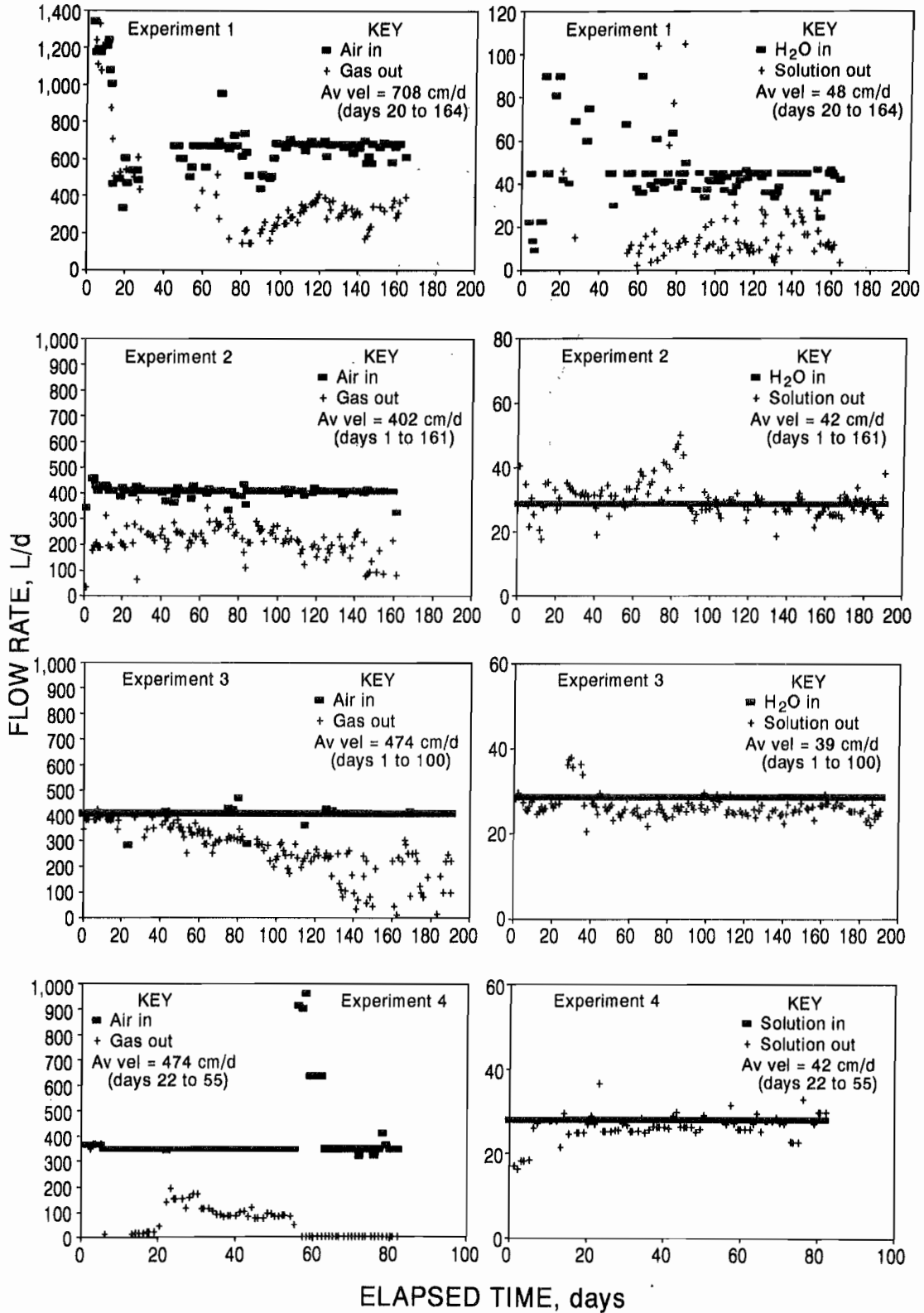
The observed  $\text{CO}_2$  gas production for experiment 1 (figure 7) appears to follow a different pattern in time than the  $\text{O}_2$  and other leach products. Its peak concentration is 20 times less than that for the peak  $\text{O}_2$  consumption and occurs 40 days sooner. There are several possible sources for  $\text{CO}_2$  during leaching: (1) reaction of acid with carbonate in the sample, (2) decarboxylation of coal, (3) low-temperature oxidation of coal, and (4) a product of bacteria metabolism. On the basis of the few data points obtained for the most probable number (MPN) of iron-oxidizing bacteria in the lixiviant at station 7 (figure 8), the bacteria population may have peaked at 80 days, which is near the minimum in  $\text{CO}_2$  concentration.<sup>8</sup> This observation would not be consistent with bacteria being a significant factor in producing the  $\text{CO}_2$  observed during the

<sup>8</sup>This interpretation of MPN data must be considered highly speculative because of the fact that MPN measurements made with sampled lixiviant may not be representative of the bacteria concentration in the column. Live bacteria generally adhere strongly to solid surfaces and do not necessarily equilibrate with their number in the lixiviant.

**Figure 2**

**Experiment 1:  $O_2$  consumption within column. (GC = gas chromatograph.)**

Figure 3



Gas (left) and liquid (right) flow rates for experiments 1 to 4.

Table 5.—Experiments 1 to 4: experimental curve-fit parameters<sup>1</sup>

$$\left[ \text{Concentration} = \frac{(D + nx)e^{-[A(t-t_0)^2]} + B}{C} ; t_0 = t'_0 [1 + c e^{-x/t}] \right]$$

Parameters <sup>2</sup>	Experiment 1				Experiment 2				Experiment 3				Experiment 4			
	O <sub>2</sub> consumed μmol/L (gas)	SO <sub>4</sub> <sup>2-</sup> μmol/L (sol)	FeD <sup>3</sup> μmol/L (sol)	H <sup>+</sup> μmol/L (sol)	O <sub>2</sub> consumed μmol/L (gas)	SO <sub>4</sub> <sup>2-</sup> μmol/L (sol)	FeD <sup>3</sup> μmol/L (sol)	H <sup>+</sup> μmol/L (sol)	THC <sub>4</sub> μmol/L (sol)	SO <sub>4</sub> <sup>2-</sup> μmol/L (sol)	H <sup>+</sup> μmol/L (sol)	FeD <sup>3</sup> μmol/L (sol)	O <sub>2</sub> consumed μmol/L (gas)	SO <sub>4</sub> <sup>2-</sup> μmol/L (sol)	FeD <sup>3</sup> μmol/L (sol)	
A	0.0025	0.0025	0.0025	0.0025	0.0012	0.0006	0.0015	0.0022	0.0006	0.001	0.003	0.006	0.006	0.006	0.007	
B	0.02	0	0	0.4	0	0	0.4	0	0	0.3	0.3	0	0	0		
C	0.00008	0.00006	0.00007	0.0005	0.00009	0.0005	0.00045	0.03	0.0048	0.005	0.015	0.00006	0.00007	0.0025		
D	0.75	6	6	6	0.75	6	0.2	0.2	0.21	0.21	0.21	0.5	5	5		
j	8.5	8.5	8.5	8.5	14.3	16	12	15	13	10.5	7	7	7	7		
k	255	255	255	275	280	325	275	260	460	500	400	100	100	100		
t' <sub>0</sub>	72	72	72	42	35	45	42	35	70	85	75	20	20	22		
n	-0.13	1	1	1	-0.13	2	1	-0.02	1	1	1	-0.1	2	2		

Sol Solution.

<sup>1</sup>x = feet measured from top of column (1 ft = 0.3048 m); t = elapsed days measured from start of column leaching.

<sup>2</sup>List of parameters refers to curve-fit equation for concentration.

<sup>3</sup>FeD refers to total dissolved iron concentration, which in the presence of O<sub>2</sub> in the gas phase is almost exclusively Fe<sup>3+</sup> ion.

Figure 4

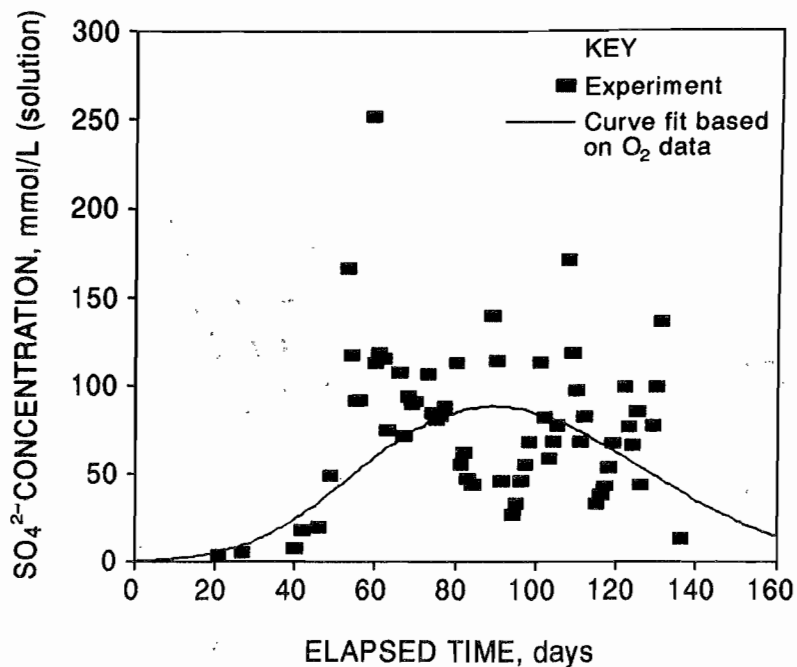
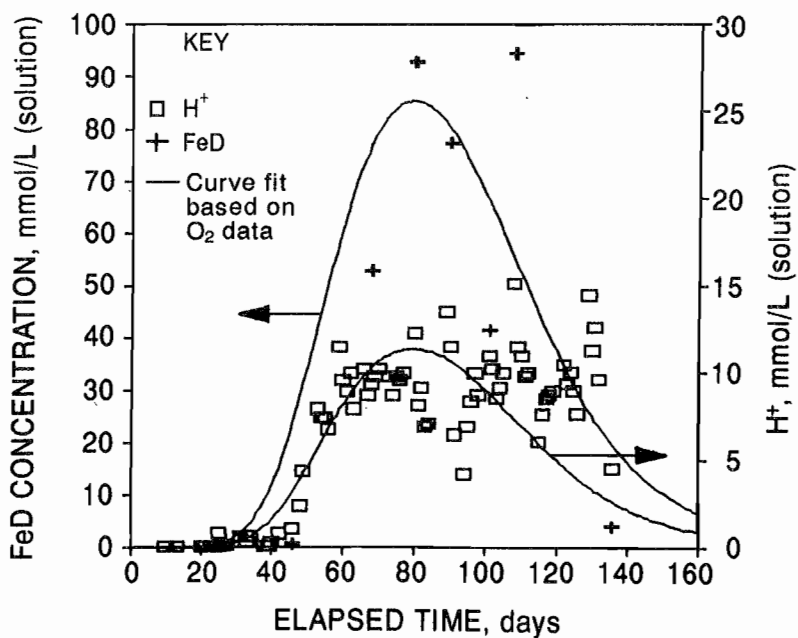
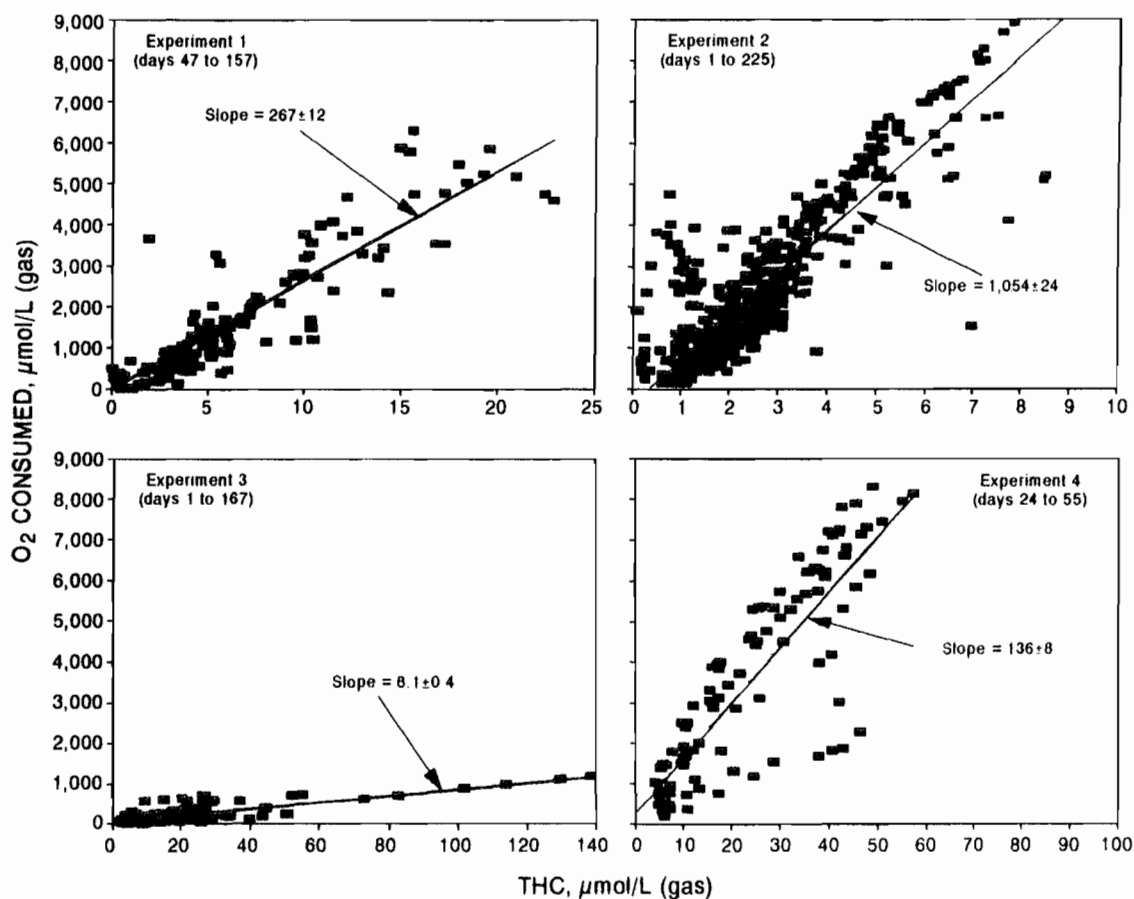
Experiment 1:  $\text{SO}_4^{2-}$  concentration in lixiviant solution at station 7.

Figure 5

Experiment 1:  $\text{Fe}^{3+}$  and  $\text{H}^+$  concentration in lixiviant solution at station 7. ( $\text{FeD}$  = total dissolved iron concentration, which in the presence of  $\text{O}_2$  in the gas phase is almost exclusively  $\text{Fe}^{3+}$  ion.)

**Figure 6****Experiments 1 to 4: correlation of THC with O<sub>2</sub> consumption.**

160-day period. The itemized CO<sub>2</sub> sources, 2 and 3 above, would represent competitive reactions for consumption of O<sub>2</sub>, in which case the CO<sub>2</sub> might decrease as the other leach products increase. However, the observed downward trend in concentrations at a later elapsed time would tend not to favor such an explanation. On the other hand, itemized CO<sub>2</sub> source 1 would depend on the acid production, which in turn would depend on the oxidation of pyrite. In this case, the decrease of CO<sub>2</sub> with time would suggest decreasing availability of unreacted carbonate content in the waste, possibly due to surface armoring by precipitated iron oxides-sulfates (15). This latter explanation would suggest a buffered H<sup>+</sup> concentration to be the cause of the apparent lag time to reaction. This possibility was investigated further in experiment 3 where a coal having a low-carbonate content was leached.

#### DATA OF EXPERIMENT 2

Experiment 2 was a repeat of experiment 1, except that air and water flows were more carefully controlled and the liquid sampling improved. Both these objectives were achieved to a degree, as can be seen from figure 3, which depicts the flows; from figure 9, which depicts the sulfate concentration; and from figure 10, which depicts the O<sub>2</sub> consumption. Figures 9 and 10 reveal that the overall shape of the curves are similar to those of experiment 1; however, the curves apparently do not exhibit the lag time prior to leaching. The peak of the O<sub>2</sub> consumption and sulfate production occurs at about day 35.

As mentioned previously, the same basic curve-fit function used for O<sub>2</sub> consumption in experiment 1 is applicable to the experiment 2 data. The specific parameters

Figure 7

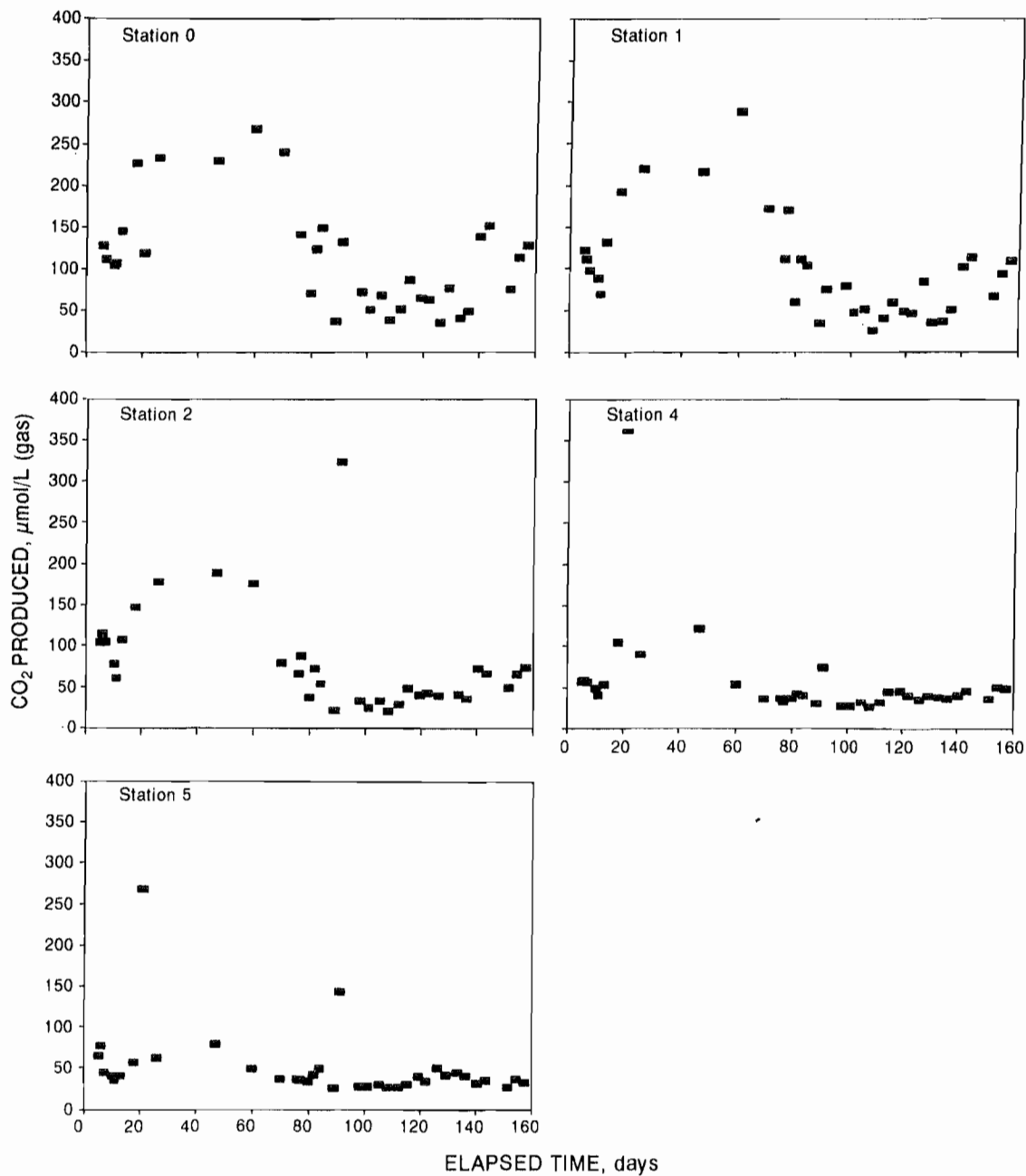
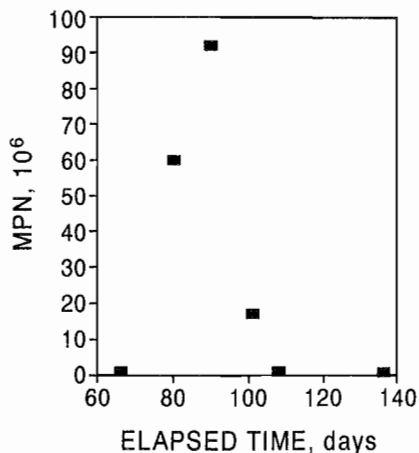
*Experiment 1: CO<sub>2</sub> gas production within column.*

Figure 8



**Experiment 1: most probable number (MPN) of bacteria measurement for lixiviant solution at station 7.**

for the gaseous components,  $\phi(x,t)$ , and for the liquid components,  $\psi(x,t)$ , are given in table 5. The various curve-fit parameters yield quite reasonable representations of the data, as can be seen in figures 9 and 10 for  $\text{SO}_4^{2-}$  concentration and  $\text{O}_2$  consumption, respectively, for  $\text{H}^+$  and  $\text{Fe}^{3+}$  concentrations compared to the  $\text{SO}_4^{2-}$  concentration at station 7 in figure 11, and for THC at station 0 in figure 12.<sup>9</sup>

As in experiment 1, the  $\text{CO}_2$  data appear to follow a different path in time (figure 13). Carbon dioxide concentrations are one to two orders of magnitude less than the observed  $\text{O}_2$  consumption, with a minimum in the curve-fit expression occurring about the time of the peak in the other leach data (i.e., 40 days). In this latter regard, it appears that relative to experiment 1, the  $\text{CO}_2$  data, like the other leach constituents, have been shifted forward in time by about 40 days. Weathering of the waste offers an explanation for the time shift, in that leach reactions would have started prior to introducing the sample into the column. Hence, acids would have already been formed and carbonate rocks already prearmored, at least to some extent.

It also appears from the few data available on MPN (figure 14), that as in the case of experiment 1, bacteria metabolism may not be a major source for  $\text{CO}_2$  production, at least over the elapsed period of 225 days.

<sup>9</sup>Solution component data at stations other than station 7 are relatively meager and their inclusion here at this time would not be very meaningful. On the other hand, the gas data on THC and  $\text{CO}_2$  are as extensive as those on  $\text{O}_2$  and are included here in their entirety.

### DATA OF EXPERIMENT 3

Experiment 3 was to examine the effects of a low carbonate content on the onset of leaching of the pyrite. The leached material in this experiment was 85.5 kg of specially cleaned Pittsburgh seam coal (table 3) that was available through the U.S. Department of Energy's Pittsburgh Energy Technology Center. Unfortunately, the degree of leaching observed with this material, in terms of measured reactant and product concentrations, was about 20 times less than with the coal waste, which posed serious constraints on the reliability of all the concentration measurements. This is readily apparent from the scattering of data in figures 15 through 18, which depict the  $\text{O}_2$  consumption and concentrations of  $\text{SO}_4^{2-}$ , THC, and  $\text{H}^+$ , respectively, as displayed in the usual manner. In addition to the problem of scattered data, and probably partially responsible for the scatter, was the fact that gas flow decreased during the experiment (figure 3). In fact, it appears that only the data at station 7 (liquids) and at station 0 (gases except for  $\text{O}_2$ ) are useful for curve-fit analysis.<sup>10</sup>

Concentration of leachate components are about a factor of 30 less than in experiments 1 and 2. However, the same basic curve-fit expression used previously seems to be applicable to some of the data of experiment 3; namely, the  $\text{SO}_4^{2-}$ ,  $\text{H}^+$ , and  $\text{Fe}^{3+}$  concentrations (figures 16, 18, and 19, respectively). The THC and  $\text{CO}_2$  gas data at station 0 (figures 17 and 20, respectively) apparently do not follow the same type of basic curve fit. Little information can be gotten from the  $\text{O}_2$  data (figure 15) other than that the quantity of  $\text{O}_2$  consumed is about twice that required if all the  $\text{CO}_2$  was produced by carbon oxidation versus decarboxylation of carbonate rock (or coal). This amount of  $\text{O}_2$  consumed appears adequate to account for the  $\text{SO}_4^{2-}$  produced, but because of the data scatter, the time variation of  $\text{O}_2$  consumed does not define a curve. However, at the same time, the scatter does not negate the possibility that the  $\text{O}_2$  dependency of the leaching process with time was actually similar to the other experiments.

### DATA OF EXPERIMENT 4

In experiment 4, 153 kg of fresh coal waste obtained from the same original source as in experiment 1 (table 4) was leached using an input lixiviant consisting of an aqueous solution of approximate 500 ppm or mg/L iron as  $\text{FeCl}_3$  (about 9,000  $\mu\text{mol}$  of  $\text{Fe}^{3+}$  per liter of solution).

<sup>10</sup>Analysis of gases by standard gas chromatography has a lower limit of detection of about 1 to 10 ppm and an uncertainty of about 2 pct of the full-scale reading. For the case of  $\text{O}_2$  consumption in experiment 3, which is determined by difference, the uncertainty becomes quite significant, on the order of  $\pm 50 \mu\text{mol/L}$  or 50 to 100 pct of the values shown in figure 15.

Figure 9

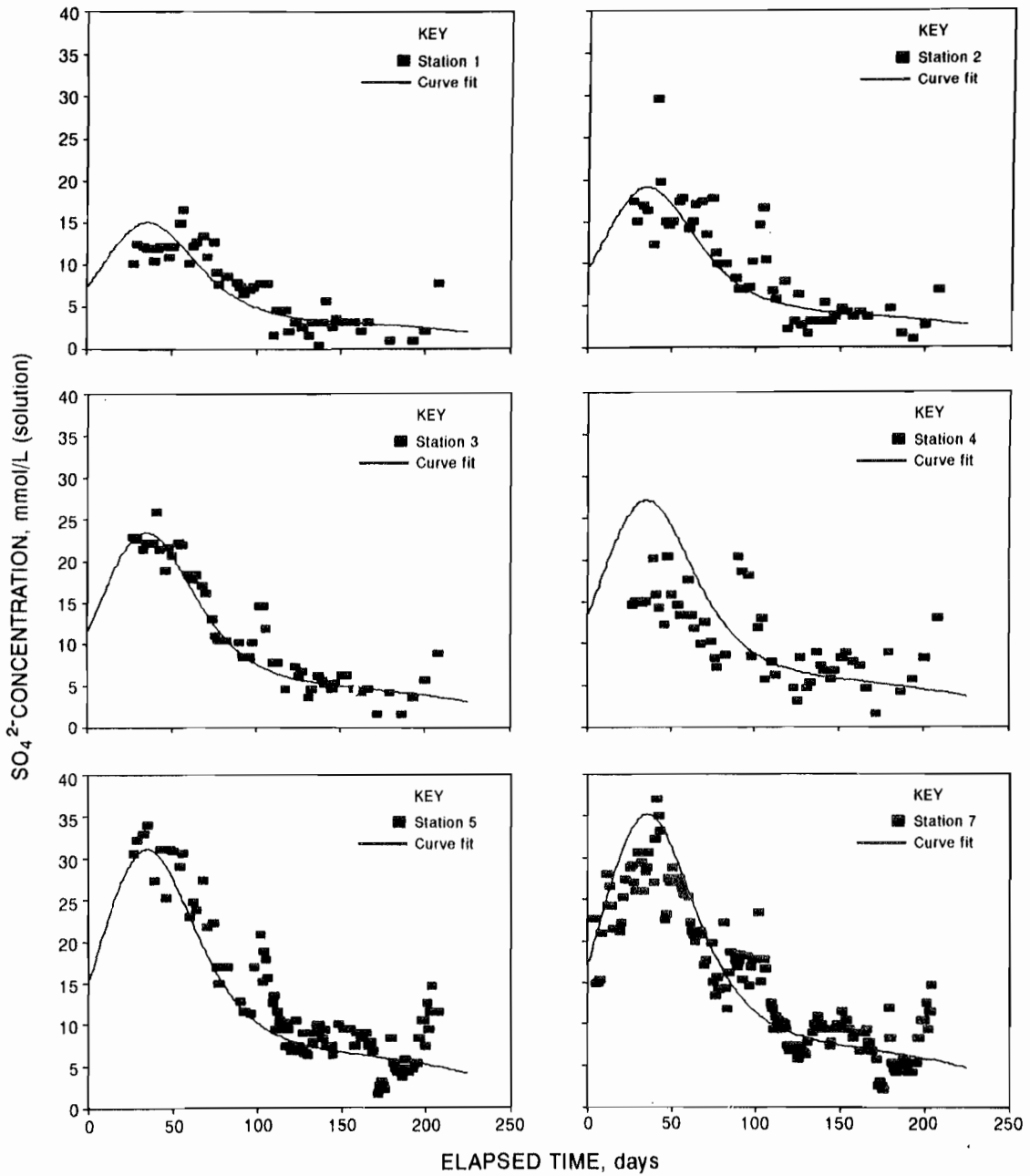
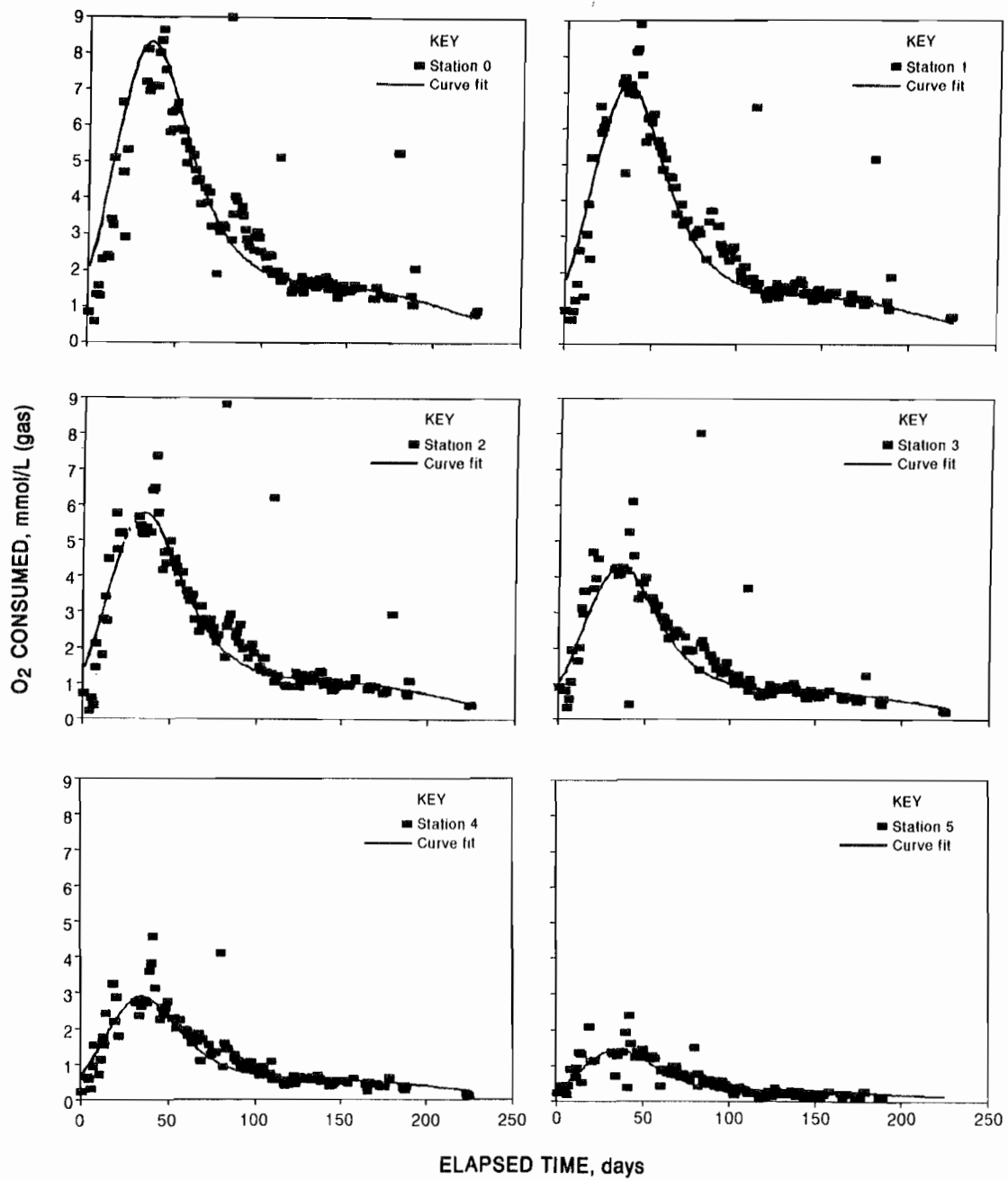
Experiment 2:  $\text{SO}_4^{2-}$  concentration in lixiviant solution.

Figure 10



Experiment 2:  $O_2$  consumption within column.

Figure 11

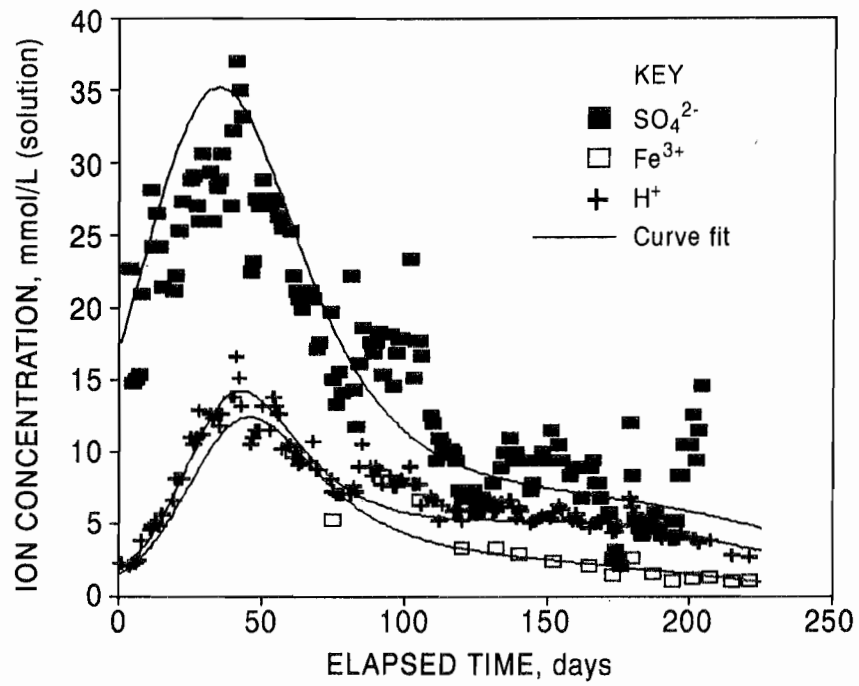
*Experiment 2: ion concentrations in lixiviant solution at station 7.*

Figure 12

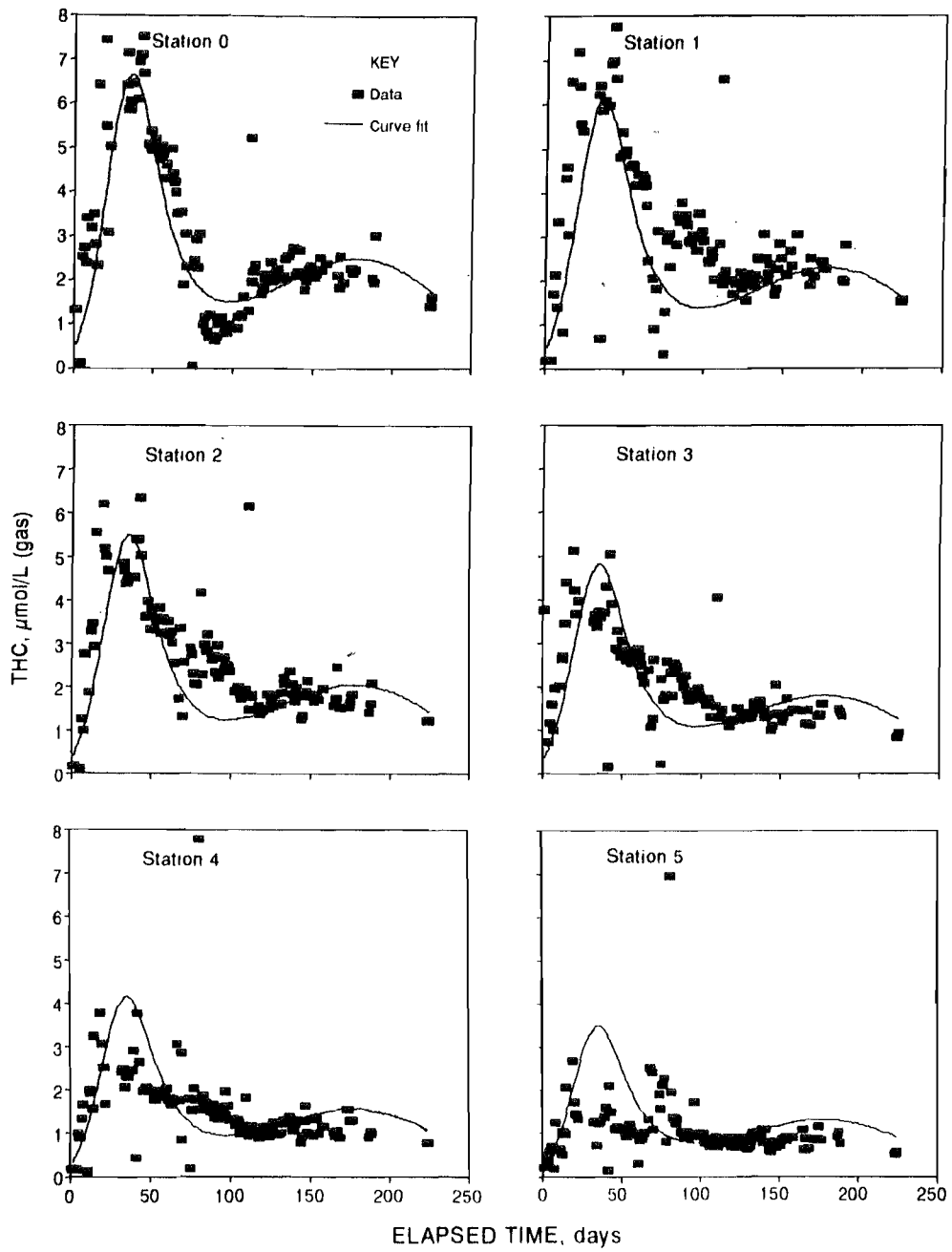
*Experiment 2: THC within column.*

Figure 13

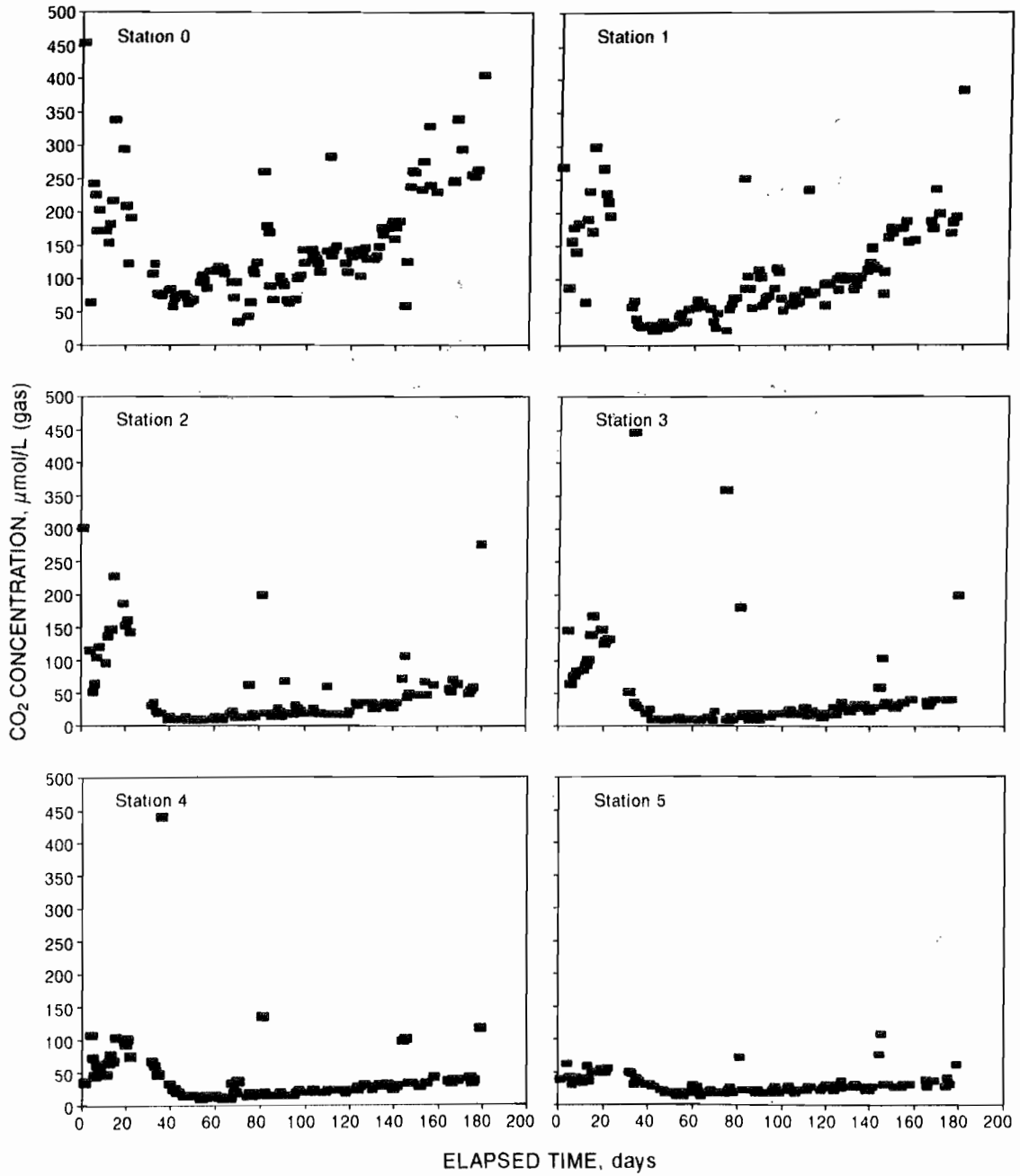
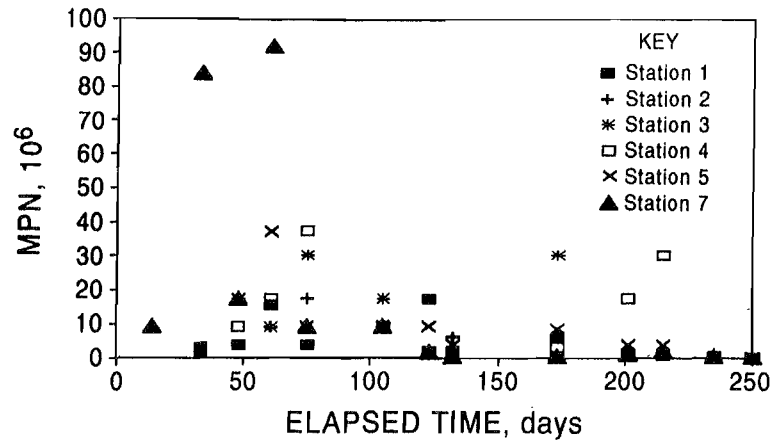
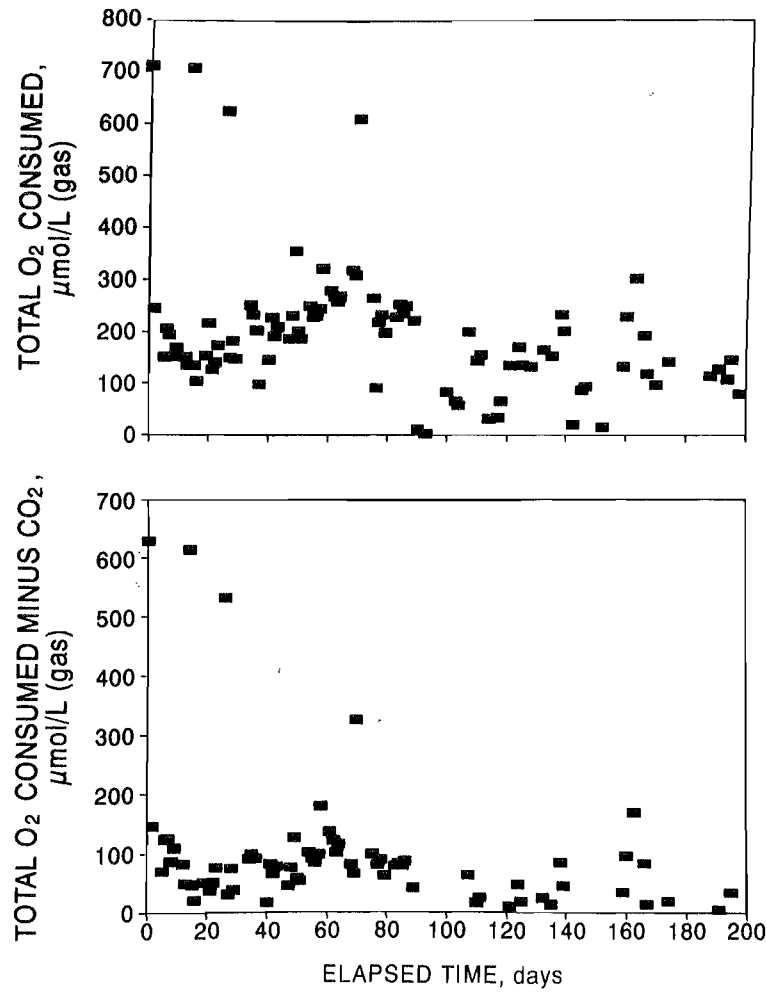
Experiment 2: CO<sub>2</sub> gas concentration within column.

Figure 14



Experiment 2: most probable number (MPN) of bacteria measurement for lexiviant solution within column.

Figure 15



Experiment 3: total O<sub>2</sub> consumption and O<sub>2</sub> consumption for other than CO<sub>2</sub> at station 0.

Figure 16

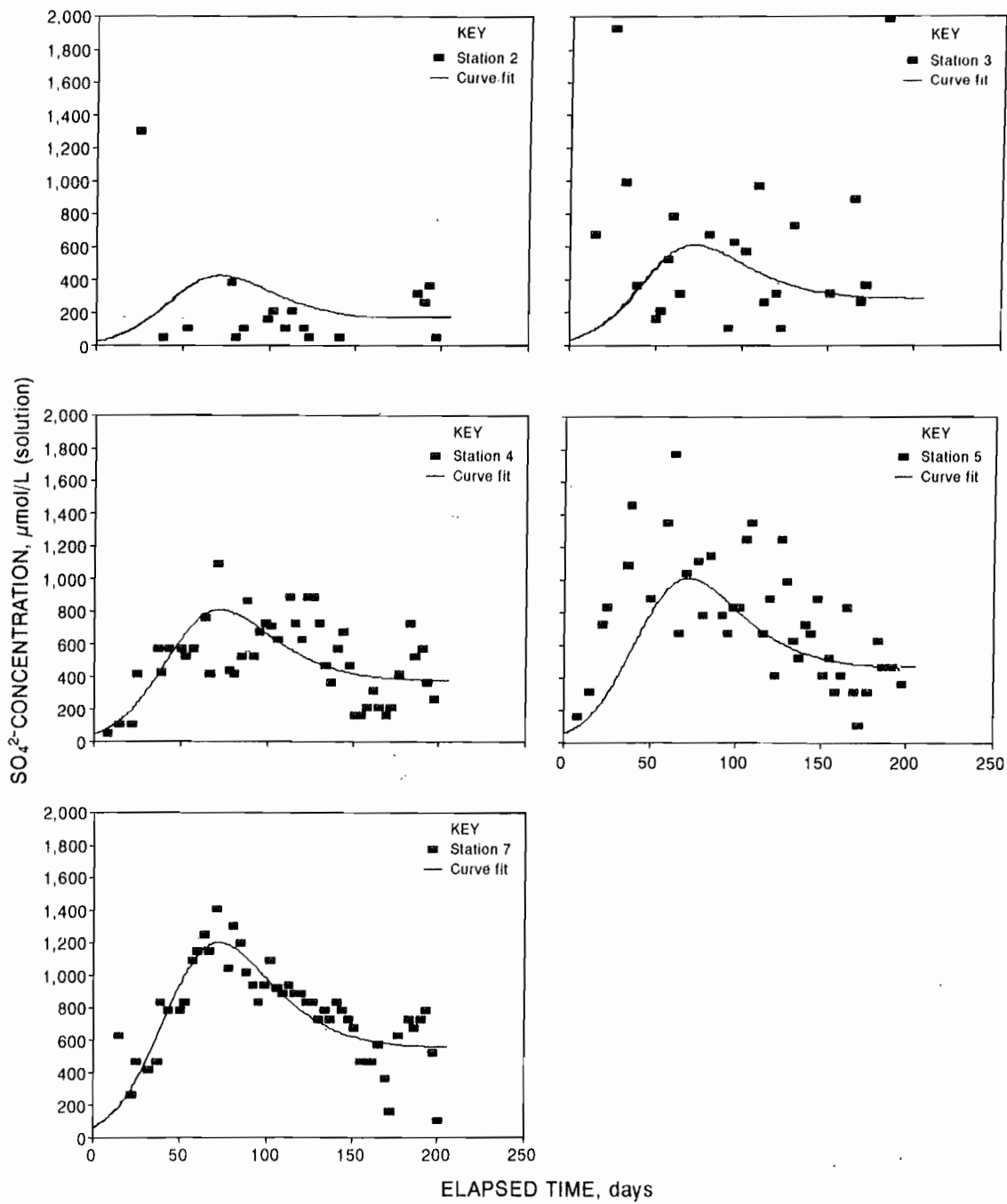
Experiment 3:  $\text{SO}_4^{2-}$  concentration in lixiviant solution.

Figure 17

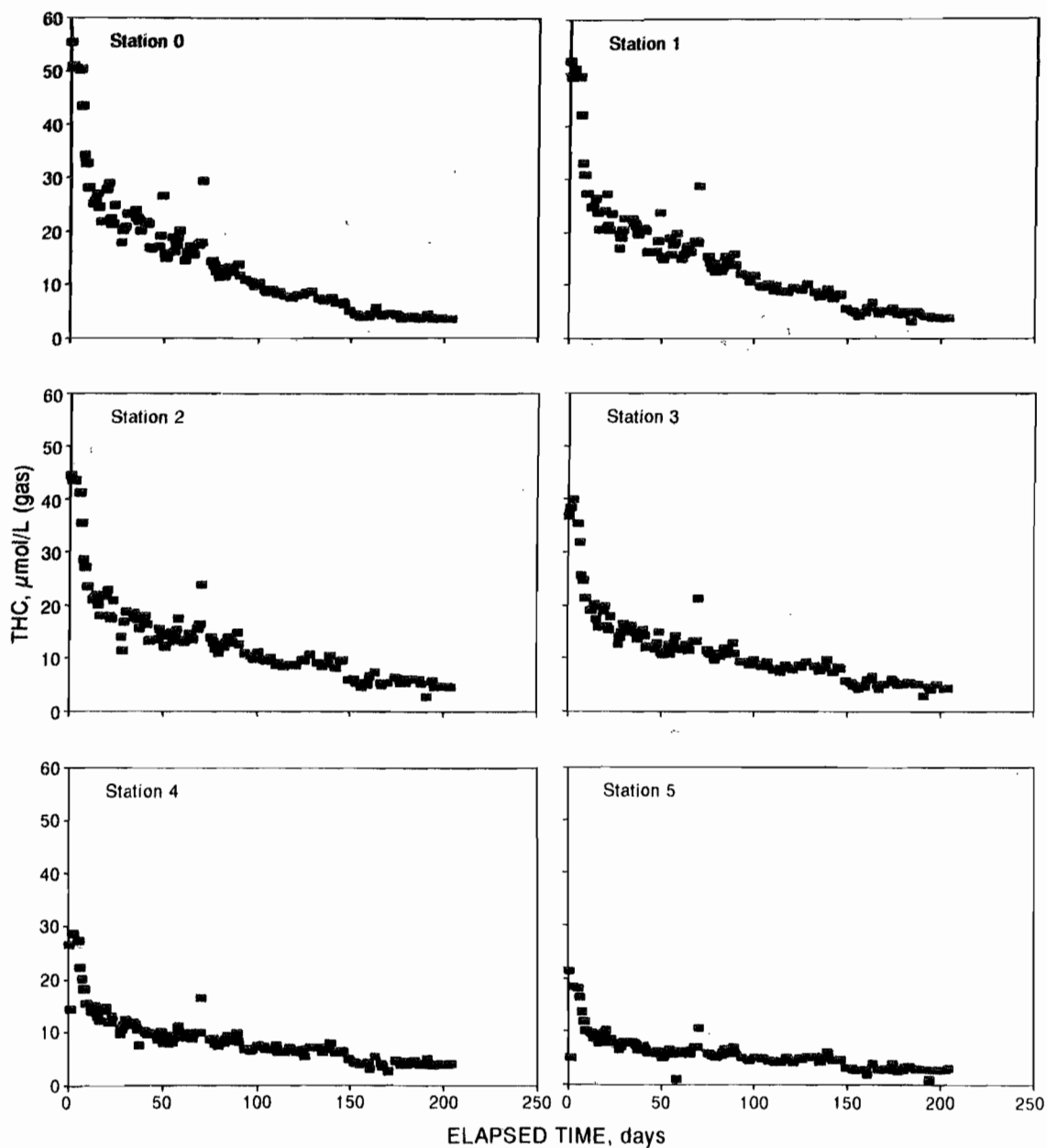
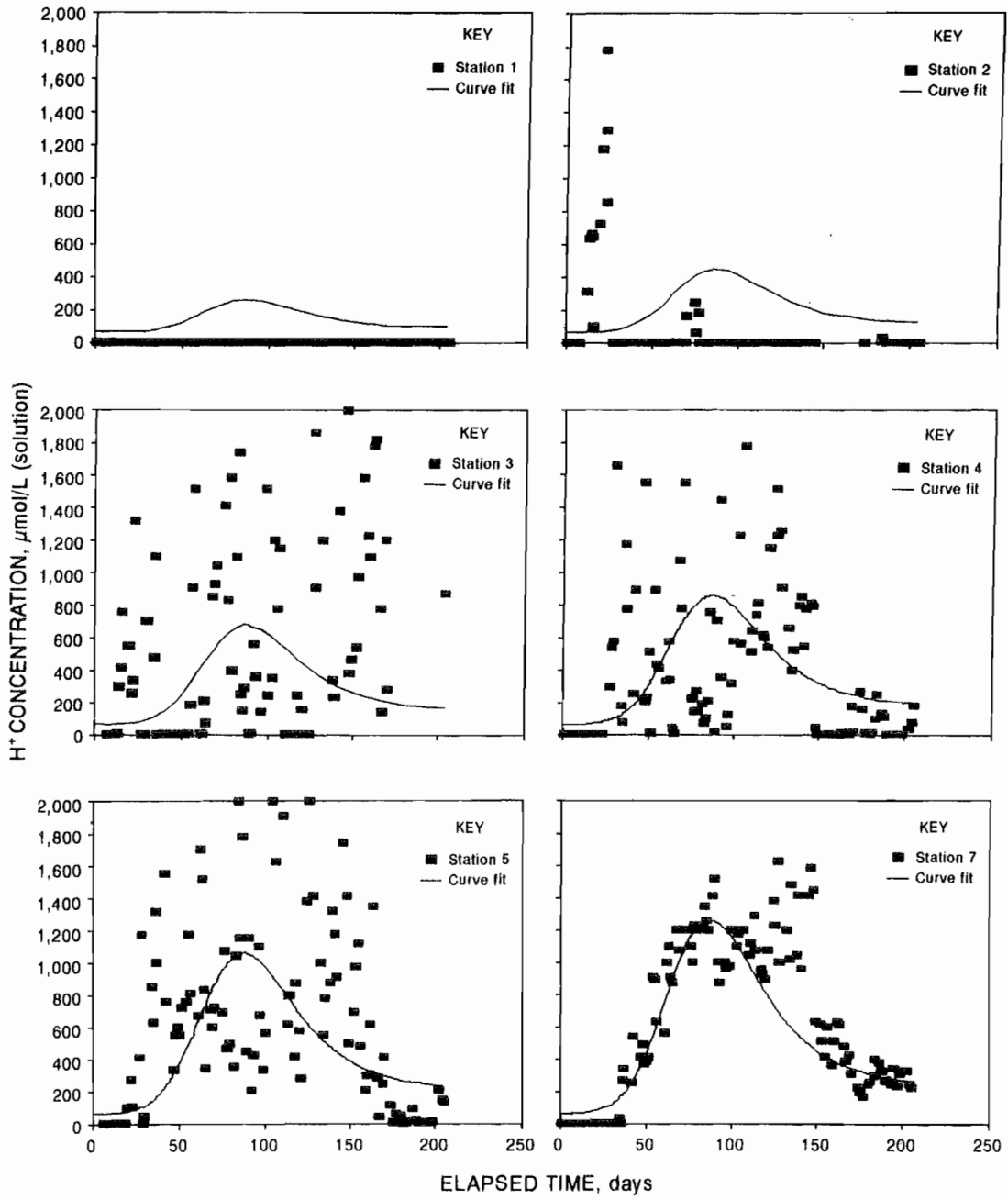
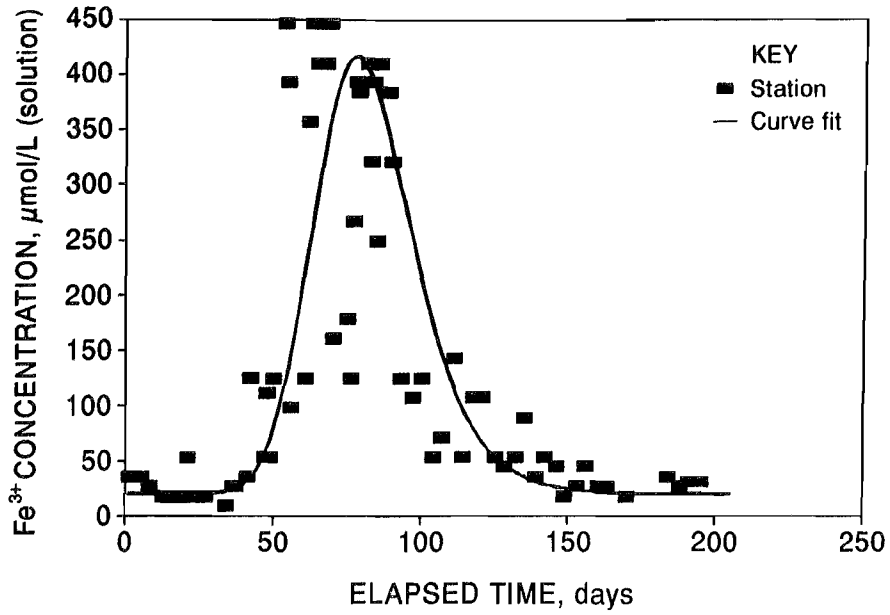
*Experiment 3: THC within column.*

Figure 18



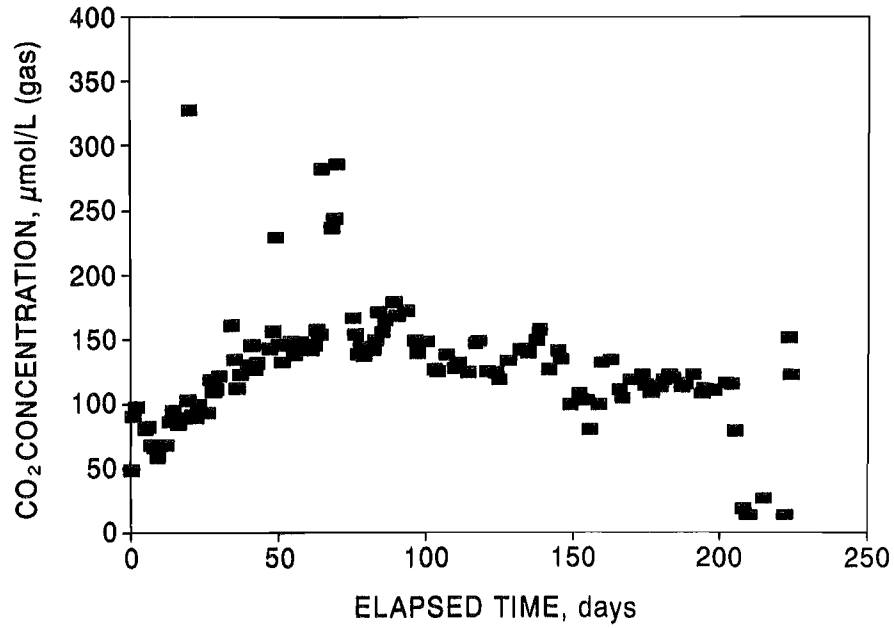
Experiment 3: H<sup>+</sup> concentration in lixiviant solution.

**Figure 19**



**Experiment 3: Fe<sup>3+</sup> concentration in lixiviant solution at station 7.**

**Figure 20**



**Experiment 3: CO<sub>2</sub> gas concentration at station 0.**

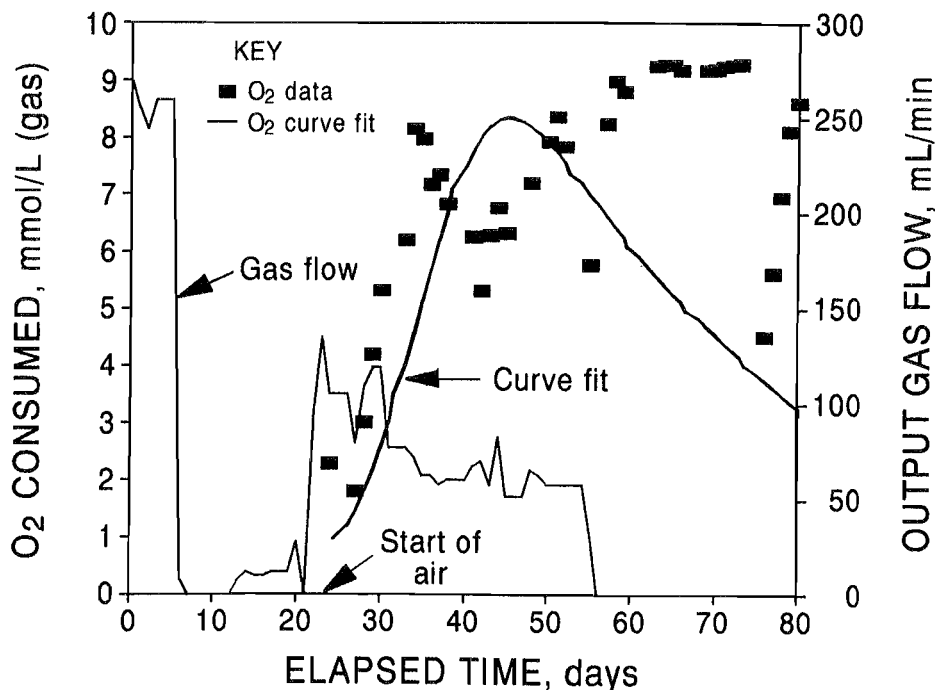
Unlike the previous experiments, bottled  $N_2$  gas was counterflowed into the column for the first 22 days; after which time, room air supplanted the  $N_2$ . It was hoped to examine three effects with these experimental conditions. First, it was thought that the  $FeCl_3$  would inhibit bacterial growth, hence rendering the leaching process abiotic. Second, it was hoped to examine the direct oxidation of pyrite by  $Fe^{3+}$  in the absence of  $O_2$  (equation 7). Third, it was hoped that the  $Fe^{3+}$  would significantly increase the rate of pyrite leaching. While the leach data apparently reflected these effects to a degree, it was clear that the different experimental conditions also had a significant effect on the leach process. Reddish precipitates formed in the column during both the  $N_2$  and air flows. Difficulties were experienced in consistently obtaining samples through the liquid probes, and the output gas flow varied with time, essentially ceasing after day 55, even though air was still being input to the bottom of the column (figure 3).

Figure 21 shows the variation of  $O_2$  consumption at station 0 superimposed on the output gas flow. It is easy to see that a curve fit of the  $O_2$  data beyond day 55 would not be meaningful. Instead, the curve fit, as shown in figure 21, is actually that for sulfate after adjusting the appropriate proportionality constants to the  $O_2$  values (table 5). This curve fit does agree reasonably well with the  $O_2$  data up to the time (day 55) of zero gas output at the top of the column. After day 55, it is most probable that

$O_2$  consumption is affected more by loss of gas from the system than by pyrite oxidation, thus negating the utility of that data. This gas loss effect is also evident from the observations at the other gas sampling stations (figure 22). As the modified sulfate curve-fit expression shown in figure 22 indicates, the correlation between sulfate production and  $O_2$  consumption is probably similar to that observed in the previous coal waste experiments. Also depicted in figure 22 are the  $CO_2$  and THC generated within the column. They too are apparently consistent with the previous experiments. As can be seen from figure 6, the correlation between  $O_2$  consumption and THC can be considered linear with a slope of about 140 mol of  $O_2$  per mole of hydrocarbon gas. This is somewhat less than that observed for experiment 1 (slope of 270) and for experiment 2 (slope of 1,050), but still a factor of 20 higher than the corresponding value (slope of 8) for the coal in experiment 3.

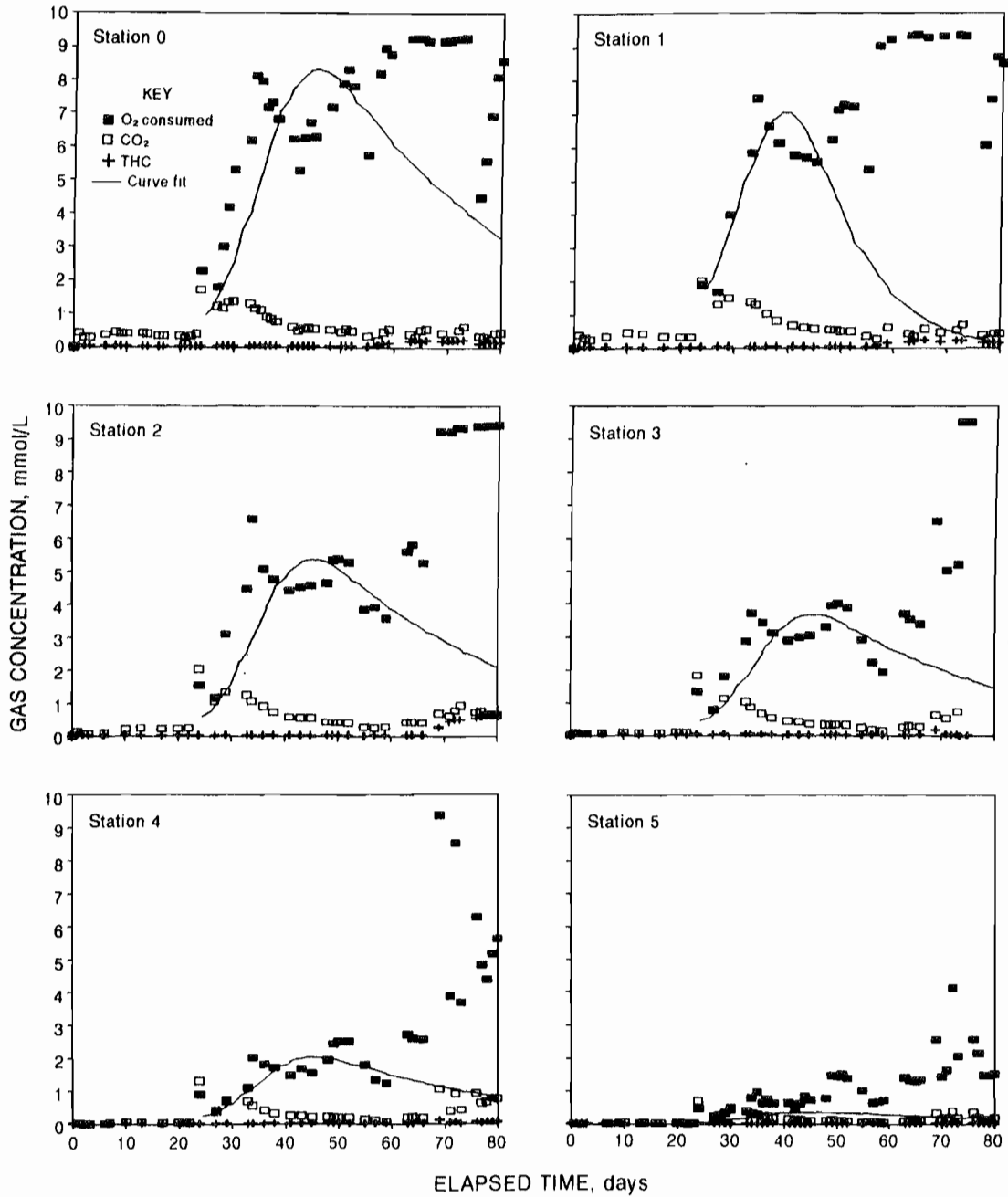
The ion concentrations from station 7 are shown in figure 23, along with the curve fits to the  $SO_4^{2-}$  and net  $Fe^{3+}$  concentrations. The net ferric data represent the measured values of  $Fe^{3+}$  minus the value of  $Fe^{3+}$  in the input lixiviant (average of  $9,100 \mu\text{mol/L}$ ). The ion concentrations beyond day 55 appear to be better behaved than the gas data in keeping with the near constant liquid flow rate (figure 3). This suggests that although the measured gas output flow rate may have decreased to zero after day 55

Figure 21



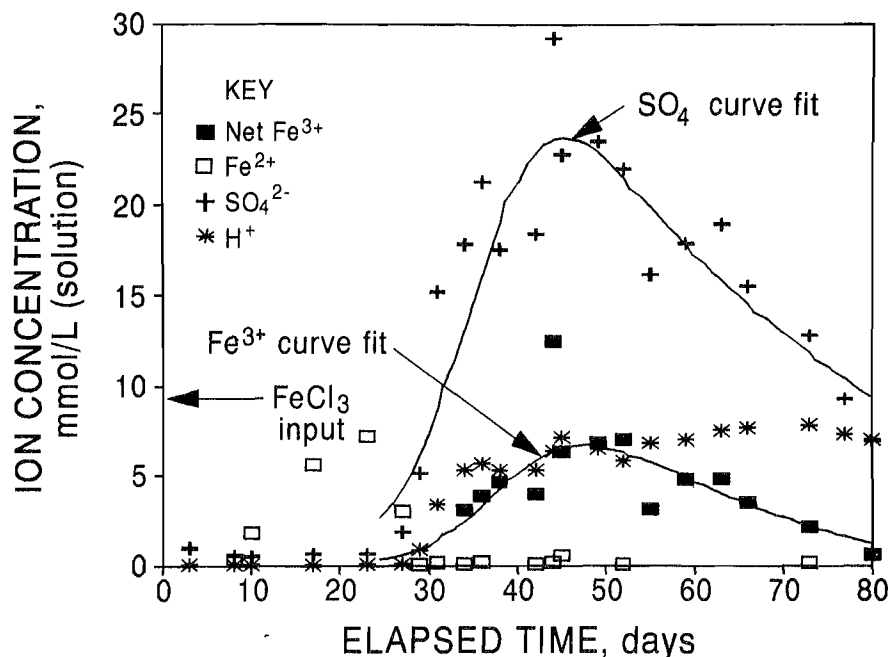
Experiment 4:  $O_2$  consumption and gas flow rate at station 0.

Figure 22



Experiment 4: gas concentrations within column.

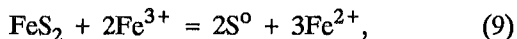
Figure 23



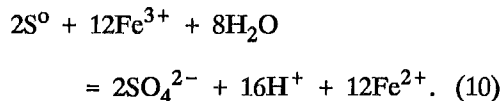
Experiment 4: ion concentrations in lixiviant solution at station 7.

(presumably because of air leakage), there was sufficient  $O_2$  input to the column to sustain the leaching processes, which then apparently decreased in the same manner as in the previous column experiments.

As shown in figure 23, during the time period of  $N_2$  gas flow (days 0 to 22), input  $Fe^{3+}$  was reduced to  $Fe^{2+}$ , but with minimal sulfate and acid appearing in the solution at station 7. The appearance of reddish precipitates in the column during this time period could be indicative of the known oxidizing potential of  $Fe^{3+}$ , e.g., as in the reactions depicted by the following equations:



and



Precipitation of iron sulfate salts (e.g., jarosites), combined with acid neutralization by carbonate rock, could account

for the absence in solution at station 7 of the  $SO_4^{2-}$  and  $H^+$  formed by these reactions.

Very shortly after  $O_2$  was admitted to the column (day 23), the pyrite leaching process became evident, much in the manner of experiment 2, which exhibited little delay to reaction compared to experiment 1, which exhibited a 35-day delay to reaction. It would appear that the initial 22 days of  $N_2$  flow may have produced the same result as the unplanned weathering of the waste sample used in experiment 2, viz, armoring of the carbonate rocks.

One liquid sample was examined for the presence of bacteria. Taken from station 7 on day 44, near the peak of the product concentration curves, the sample showed a zero MPN, suggesting that the high-chloride ion concentration (about 28,000  $\mu\text{mol/L}$ ) may have prevented bacteria from growing in the column. However, bacteria, if present, would tend to attach to the solid substrate rather than appear in the liquid efflux; although the presence of bacteria (i.e., MPN > 0) was observed in the other experiments.

## KINETIC INTERPRETATIONS

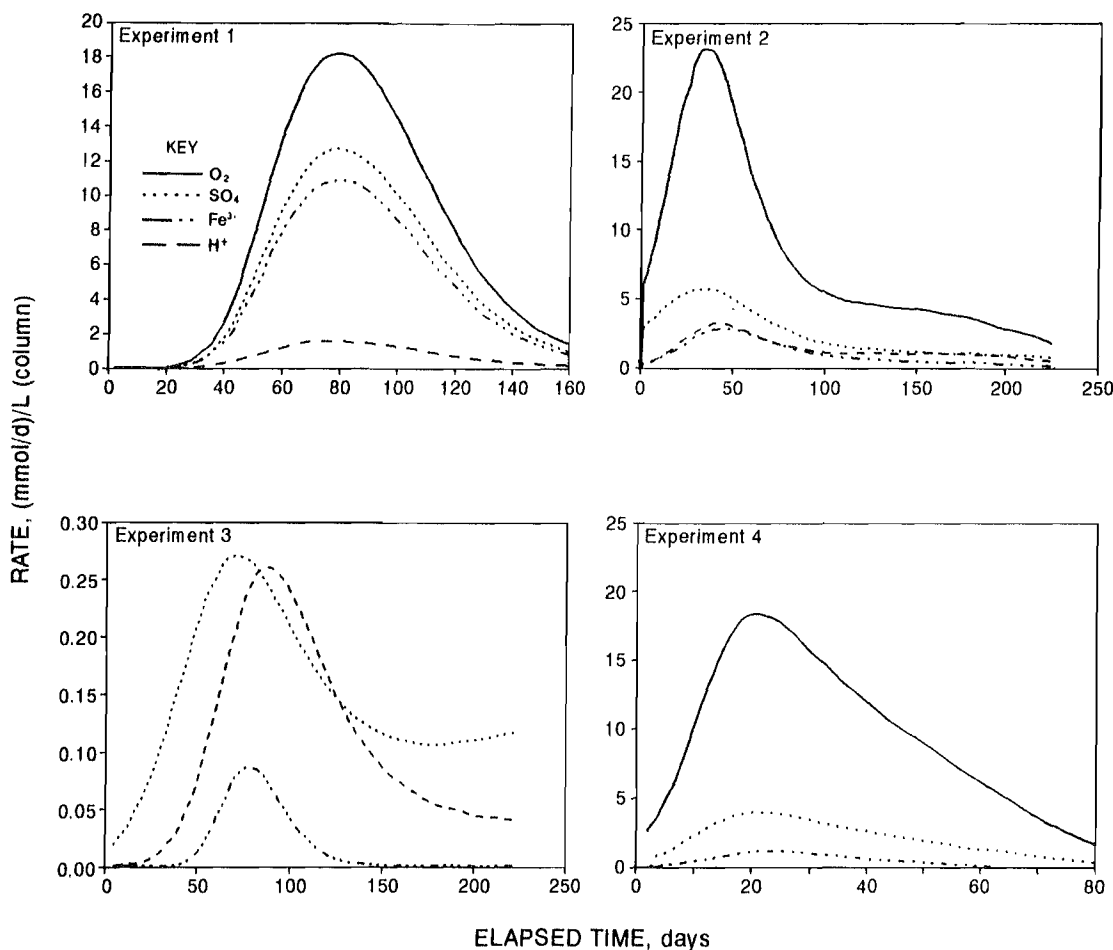
## RATES OF REACTION AND STOICHIOMETRY

Following the methodology outlined in the "Theoretical Basis" section, the curve-fit equations of table 5 were differentiated with respect to time and distance to yield those partial derivatives appearing in equation 5. Equation 5 was then solved using averaged constant flow rates (figure 3) to yield the kinetic rates of production of  $\text{SO}_4^{2-}$ ,  $\text{Fe}^{3+}$ , and  $\text{H}^+$ , and the kinetic rate of consumption of  $\text{O}_2$ . The kinetic rates obtained for each experiment, in terms of millimoles per day per liter of column volume, are shown in figure 24. Before discussing them, some explanatory comments should be made.

In experiment 1, only the  $\text{O}_2$  data were deemed sufficient to define a curve fit in time and distance—the other

species suffering from a lack of and/or excessive scatter in the data. Therefore, the curve-fit expressions for the products listed in table 5 for experiment 1 are essentially the  $\text{O}_2$  consumption curve with parameters modified *ad hoc* to be consistent with the range of experimental values observed for the product species. In the case of experiment 4, just the opposite approach was taken. The sulfate data were curve fit and its equation was then used *ad hoc* to describe the  $\text{O}_2$  data. For experiments 2 and 3, the curve-fit expressions are based on the actual data obtained for each of the product-reactant species. As shown in table 5, the same overall curve-fit function was found suitable for each of the product species, except for  $\text{CO}_2$  (figures 6, 7, 13, 20, and 22).

Figure 24



Experiments 1 to 4: rates of production of ions and consumption of  $\text{O}_2$  within column.

The rate curves shown in figure 24 for  $O_2$  consumption are based on total  $O_2$  consumed, i.e., for production of sulfate and possibly for  $CO_2$ . In view of the fact that  $CO_2$  could be produced by low-temperature oxidation of coal as well as by decarboxylation of the carbonates in the system, the rate of  $O_2$  consumption really should not be assigned exclusively to the pyrite leaching reaction. However, for the coal waste experiments (1, 2, and 4), the measured  $CO_2$  accounts for a maximum of 5 pct of the  $O_2$  consumed during the early and later stages of reaction, and at the peak, less than 1 pct. In these cases, it is reasonable to expect the  $O_2$  rate to reflect the rate of sulfur oxidation. In the case of the coal leaching (experiment 3), the measured  $CO_2$  production was a very significant fraction of the  $O_2$  consumption (as much as 50 pct). This fact, along with the considerable data scatter associated with the relatively small quantities of  $O_2$  consumed during the experiment, negates any reasonable attempt to curve fit the  $O_2$  data and accounts for the absence of the  $O_2$  curve fit from the list of results shown in table 5.

The stoichiometric ratios applicable to the pyrite leaching process would normally be given by the ratio of rates. These are plotted in figure 25, with average values shown in table 6.

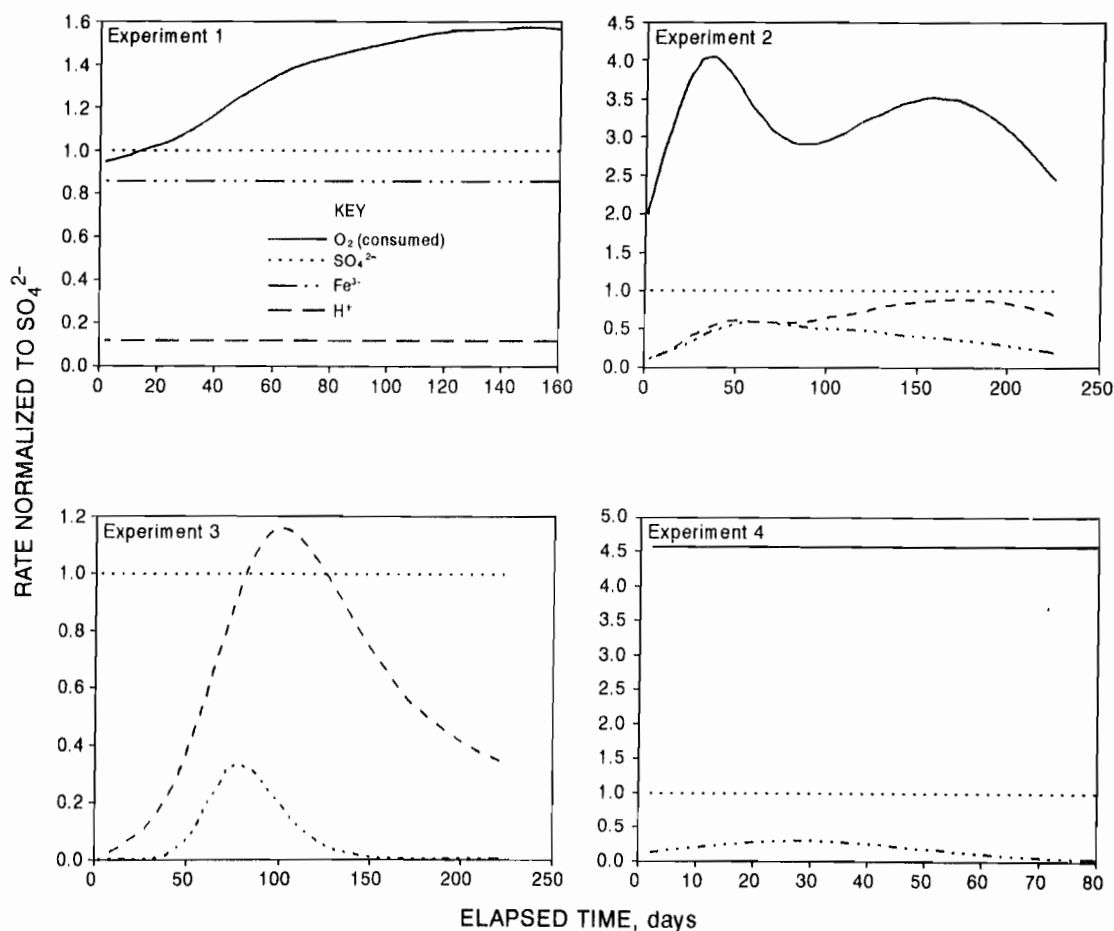
Table 6.—Averaged stoichiometric ratios

	Ratio averaged over elapsed days	Ratio relative to $SO_4^{2-}$ rate of production			
		$O_2$	$SO_4^{2-}$	$Fe^{3+}$	$H^+$
Experiment:					
1	50-150	1.4	1.0	0.9	0.1
2	10-220	3.3	1.0	0.4	0.7
3	75-125	NAP	1.0	0.2	1.1
4	10 <sup>1</sup> -32	4.6	1.0	0.3	NAP
Equation 14	NAP	1.875	1.0	0.5	0.5

NAP Not applicable.

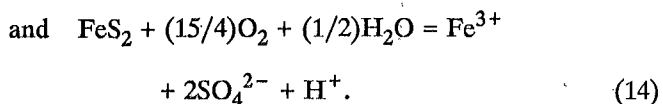
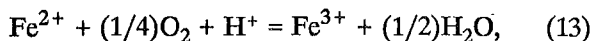
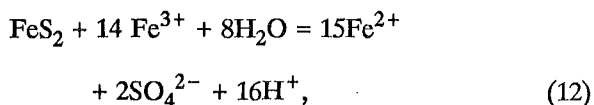
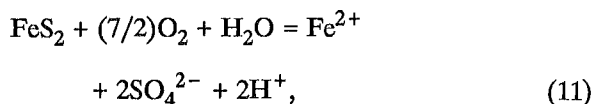
<sup>1</sup>Zero time taken when air is first introduced into the column.

Figure 25



Experiments 1 to 4: stoichiometries for  $O_2$ ,  $Fe^{3+}$ , and  $H^+$  relative to  $SO_4^{2-}$ .

Balanced reactions that have often been proposed for the pyrite oxidation process in aqueous media are:



In equation 11, dissolved  $\text{O}_2$  is the oxidant, while in equation 12,  $\text{Fe}^{3+}$  is the oxidant. Equation 13 refers to the aqueous oxidation of  $\text{Fe}^{2+}$  to  $\text{Fe}^{3+}$ , which in a cyclic process with the reaction shown by equation 12 and/or a series process with the reaction shown by equation 11 yields an overall reaction, equation 14. Stoichiometries for equation 14 relative to  $\text{SO}_4^{2-}$  are shown in the last row of table 6. The reaction given by equation 13 is known to be rapidly catalyzed by iron- and sulfur-oxidizing bacteria, such as *Thiobacillus ferrooxidans*, *Leptospirillum ferrooxidans* and *T. thiooxidans* (13). The ubiquitous nature of these bacteria would almost ensure their presence during column leaching, except perhaps in experiment 4 where the initial lixiviant contained  $\text{FeCl}_3$  (16-17).

Comparing the apparent experimental stoichiometries shown in table 6 compared to those for the balanced reactions (equations 11 to 14) gives no clear indication of the nature of the reaction process. The data do show a relatively wide variation in apparent stoichiometry from experiment to experiment, which can be explained in part by the results of the solids analysis during and after the leaching process (tables 1 to 4). In each experiment, more sulfur (sulfate and/or organic) was found in the solid phase than was present before leaching began. This can only mean that some of the sulfur-containing products of the pyrite leaching process (e.g., sulfur and iron sulfate-hydroxide salts) remained with the solid phase rather than appearing as ionic species in the liquid phase.<sup>11</sup> As can be seen in tables 1 to 4, this excess sulfur varied from 7 pct in the case

<sup>11</sup>In the ultimate analysis procedure for coal (18), organic sulfur is determined by the difference between the total sulfur value ( $\text{SO}_2$  produced by combustion) and the soluble sulfur value (in  $\text{HCl}$  for sulfate sulfur, in  $\text{HNO}_3$  for pyritic sulfur). Thus, any sulfur forms produced during leaching, but which did not dissolve during ultimate analysis (e.g., jarosites), would be interpreted as organic sulfur.

of experiment 2 to a high of 158 pct in the case of experiment 4. Two conclusions arise from these observations:

1. The stoichiometric ratios as determined from the ratio of rates of production-consumption are not very meaningful, except perhaps in the case of experiment 2 where the solids analysis indicated a relatively small amount of excess sulfur (table 2).

2. To determine a rate of oxidation of pyrite, all sulfur-containing products (i.e.,  $\text{SO}_4^{2-}$  in solution and excess sulfur in the solid) must be considered. That is, the curves of figure 24 must be corrected for the excess sulfur.

Action on this second point was carried out in *ad hoc* fashion by increasing the daily rate of sulfate production in each of the experiments by a constant factor that would lead to an accounting of the measured excess sulfur in terms of the total sulfate production (i.e., achieving a sulfur balance). The corrected rates of pyrite reaction are shown in figure 26. Figure 27 depicts the integrated form (in time) of both the corrected and uncorrected rates to yield the percentage of pyrite removal as a function of time.

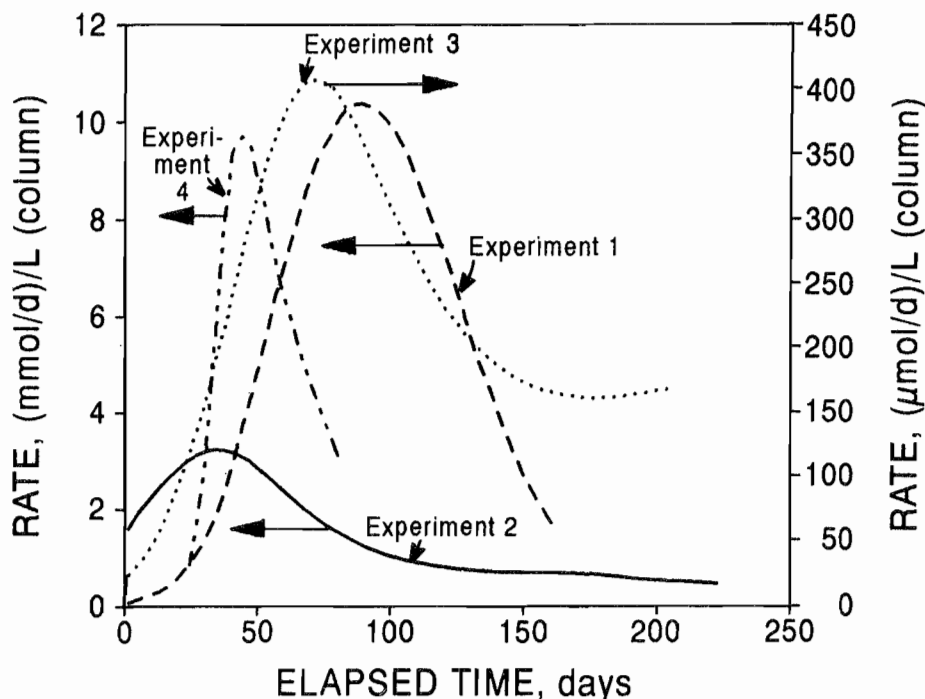
In terms of the total pyrite removed, the correction for excess sulfur is very significant for experiments 3 and 4. In all cases, the correction leads to improved agreement between the calculated and the measured percentage of pyrite removal, which ranged from about 16 pct for the coal to 30 to 70 pct for the coal waste.<sup>12</sup>

With the corrections taken to balance the sulfur, the peak pyrite reaction rates (figure 25) become very nearly the same in the case of experiments 1 and 4 (about 10 ( $\mu\text{mol/d}$ )/L of column). The peak rate for experiment 2 is about a factor of 3 slower, a difference that may not be significant in view of the uncertainty of some of the data and/or the diagnostic analysis. On the other hand, the peak rate for experiment 3 (coal) is about 25 times slower, which is probably significant. For a diffusion-limited reaction, this would imply a lower permeability for the coal relative to the coal waste.

The two experiments (2 and 4) where prereaction probably occurred have similar times to peak reaction (30 to 40 days), while the other two experiments (1 and 3) where little prereaction would have occurred have later peak times (70 to 80 days). In the case of no prereaction, the leachable solids were substantially different—experiment 1 being coal waste, with 69.3 pct ash and high-carbonate content (0.56 pct as  $\text{CO}_2$ ) (table 1), and experiment 3 being

<sup>12</sup>In the case of the coal (experiment 3), other leaching studies with this same material have yielded pyrite removals ranging from 7 to 24 pct (10-11).

Figure 26



Experiments 1 to 4: rate of reaction of pyrite within column.

coal, with 9 pct ash and relatively low-carbonate content (0.24 pct as  $\text{CO}_2$ ) (table 3). In these two cases, it would appear that carbonate content by itself did not affect the time to peak reaction nor the rate of reaction at the peak.

On the other hand, prereaction in experiments 2 and 4 apparently did shorten the time to achieve peak reaction, perhaps by partial armoring of the carbonate rock content prior to leaching. Armoring the carbonate would decrease the acid-buffering capacity of the carbonate, allowing for more rapid lowering of pH in the leachate and faster dissolution of the pyrite oxidation products. The rate of the pyrite reaction, if proportional to the  $\text{H}^+$  concentration, would be expected to increase with increasing time as the carbonate in the solid phase becomes depleted and/or armored by iron sulfate-oxide deposits. This explanation can account for the prepeak growth phase of the leach process, but by itself cannot account for the post-peak phase where the rate of reaction and the  $\text{H}^+$  concentration both decrease. Here, the carbonate armoring explanation would imply a reversal of the armoring process—an unlikely event.

#### REACTION ORDER

The discussions leading up to and following equation 6 ("Theoretical Basis" section) indicate that information on

the reaction order(s) can be determined from the concentration time-distance data. The special case mentioned of having a maximum rate within the column (i.e.,  $dR_p/dx = 0$ ) apparently did not occur in these experiments, but some significant information relative to reaction order can still be ascertained.

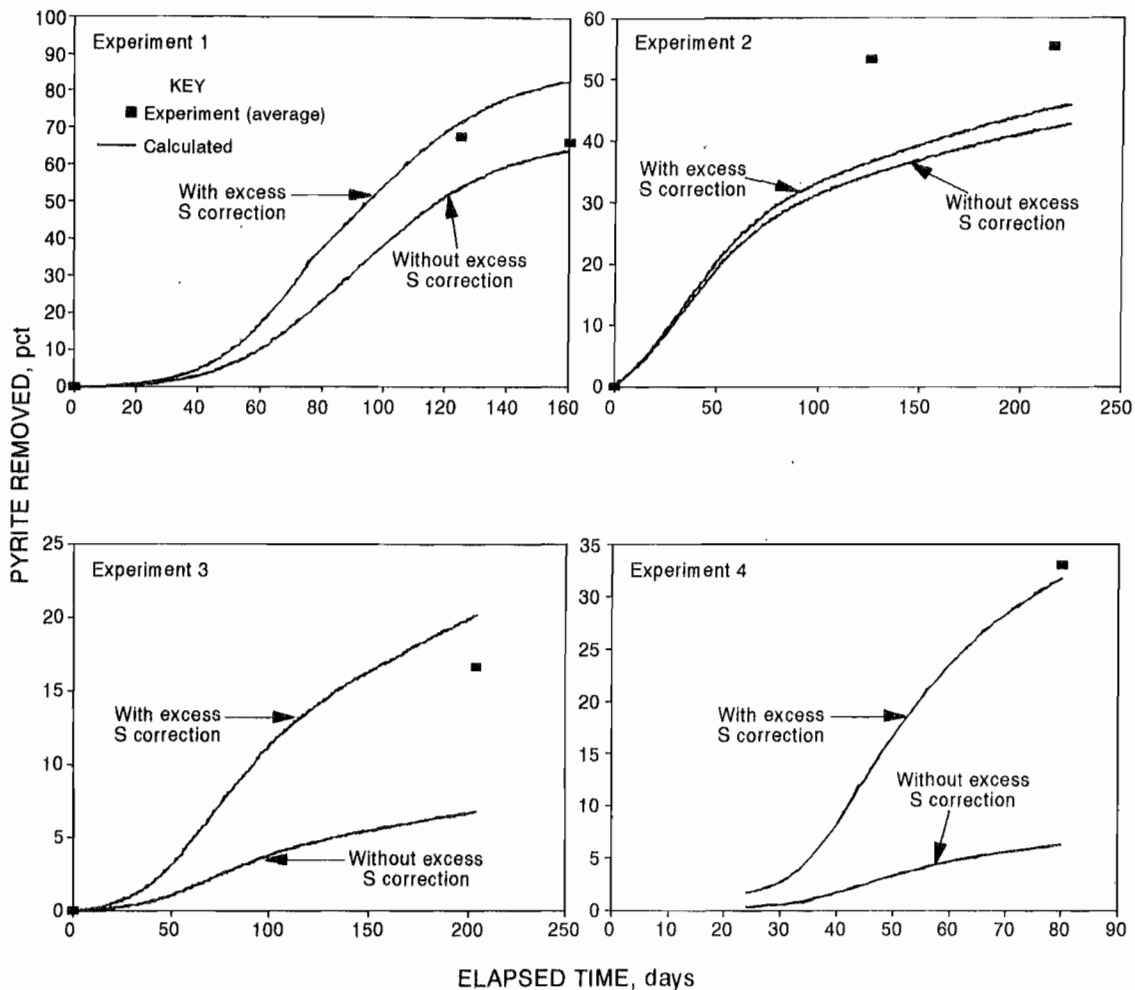
In all four experiments, considerable pyrite (30 to 85 pct) remained in the column long after the leaching rate reached its maximum and then decreased to near zero. This factor would suggest that the rate of reaction during the time of leaching may be independent of the pyrite concentration in the coal. With the assumption of zero order with respect to pyrite and all other solid-phase components, equation 2 becomes

$$R_p = k_r \alpha^{a'} \beta^{b'}, \quad (15)$$

where in the discussions to follow,  $k_r$  will be taken as independent of time,  $\alpha$  will be taken as the gaseous  $\text{O}_2$  concentration, and  $\beta$  the leachate  $\text{Fe}^{3+}$  concentration, all normalized to column volume. In accordance with reactions given by equations 11 through 14 above, these oxidants along with pyrite would be expected to be major reactant components in the leaching process.

The variation of  $R_p$  with  $\text{O}_2$  present in the column reveals a negative slope (i.e., the rate of leaching increasing

Figure 27



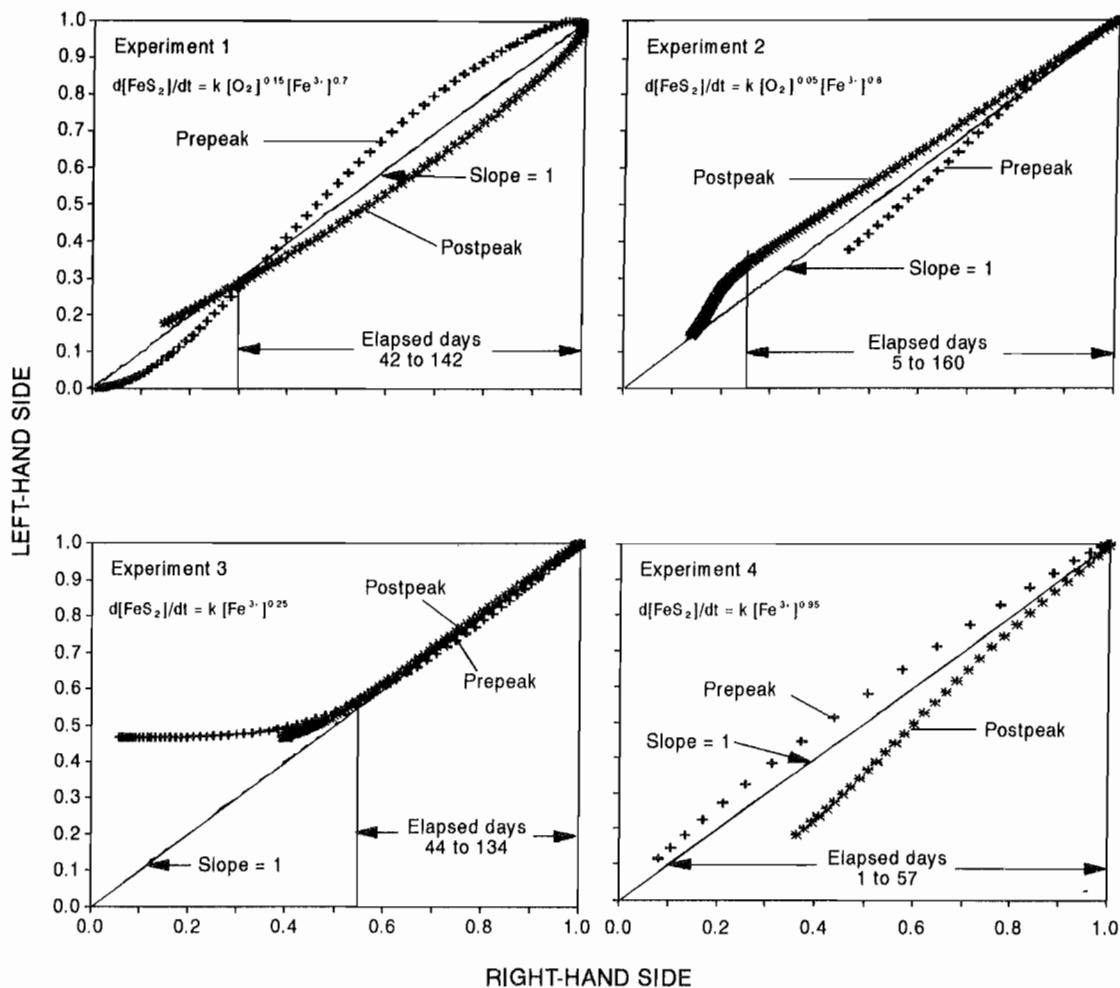
Experiments 1 to 4: extent of pyrite removal within column.

with decreasing  $O_2$ ), which is not very plausible and which indicates that the rate constant is not independent of time and/or that there must be at least one other reactant that also varies with  $O_2$ . It is interesting to examine the rate expression when  $k_r$  is constant and the other reactant is assumed to be  $Fe^{3+}$  in the leachate. This is accomplished by solving equation 15 for  $\beta$  in terms of  $R_p$  and  $\alpha$  and then evaluating the theoretical quantities in terms of the curve-fit data. For the case where  $O_2$  and  $Fe^{3+}$  are the only reactants considered, all quantities in equation 15 are known, except  $a'$  and  $b'$  and  $k_r$ . However, when  $k_r$  is taken as constant, it can be eliminated by normalizing to the peak reaction rate. This is shown in equation 16 where the rate and concentrations are normalized to their value at the reaction peak (i.e., at maximum,  $d[FeS_2]/dt = R_{p0}$ , at minimum,  $[O_2] = \alpha_0$  and at maximum,  $[Fe^{3+}] = \beta_0$ ), i.e.,

$$(\beta/\beta_0)^{b'} = (R_p/R_{p0})(\alpha/\alpha_0)^{-a'} \quad (16)$$

Values of  $a'$  and  $b'$  can now be evaluated by comparing numerical calculations of the left-hand side (LHS) of equation 16 with numerical calculations of the RHS, utilizing the curve-fit data functions in table 5 and the pyrite leaching rates shown in figure 26, to obtain values of the parameters. The best of a trial-and-error approach using graphical representations is shown in figure 28. The straight line of slope = 1 in these graphs represent the ideal case where LHS = RHS. The plotted data points are the calculated results for the specific values of  $a'$  and  $b'$  shown. It turns out that these data curves are quite sensitive to the values chosen for  $a'$  and  $b'$ , at least for values between 0 and 3. A variation of 0.05 in either  $a'$  or  $b'$  leads to a noticeable displacement of the curves

Figure 28



Experiments 1 to 4: test of reaction orders from kinetic data and concentrations.

from the ideal straight line. The data curves shown in figure 28 represent the best fit found and give rise to the empirical reaction rate expressions depicted by equations 17 to 20,<sup>13</sup> in micromoles per day per liter (column).

$$\text{Experiment 1: } R_p = 0.054 [\text{Fe}^{3+}]^{0.7} [\text{O}_2]^{0.15}. \quad (17)$$

$$\text{Experiment 2: } R_p = 0.047 [\text{Fe}^{3+}]^{0.8} [\text{O}_2]^{0.05}. \quad (18)$$

$$\text{Experiment 3: } R_p = 28 [\text{Fe}^{3+}]^{0.23}. \quad (19)$$

<sup>13</sup>In the case of experiment 3, only variations in  $b'$  were considered. Because of the paucity of  $\text{O}_2$  data,  $a'$  was simply set at zero.

$$\text{Experiment 4: } R_p = 0.052 [\text{Fe}^{3+}]^{0.95}. \quad (20)$$

Except for experiment 3, where the significance of the leaching data (particularly  $\text{O}_2$ ) and the diagnostics are most open to question, the empirical expressions do suggest a rate process that is first order with respect to  $\text{Fe}^{3+}$  and zero order with respect to  $\text{O}_2$ . The small  $\text{O}_2$  dependence shown for experiments 1 and 2 could arise from the initial stages of the leaching process when there is little  $\text{Fe}^{3+}$  available for reaction; hence, for a short time period,  $\text{O}_2$  could be the dominant oxidant. The decreasing values for  $a'$  as determined empirically for experiments 1, 2, and

4 are in the same order as the increasing values of  $\text{Fe}^{3+}$  or  $\text{Fe}^{2+}$  in the lixiviant at the start of the experiments.<sup>14</sup>

With a leaching process that is assumed first order in  $\text{Fe}^{3+}$  and zero order in  $\text{O}_2$ , the rates of reaction as evaluated from the peak rates become those given by equations 21 to 24, in micromoles per day per liter (column).

$$\text{Experiment 1: } -\frac{d[\text{FeS}_2]}{dt} = 0.0024 [\text{Fe}^{3+}]. \quad (21)$$

$$\text{Experiment 2: } -\frac{d[\text{FeS}_2]}{dt} = 0.0049 [\text{Fe}^{3+}]. \quad (22)$$

$$\text{Experiment 3: } -\frac{d[\text{FeS}_2]}{dt} = 0.0013 [\text{Fe}^{3+}]. \quad (23)$$

$$\text{Experiment 4: } -\frac{d[\text{FeS}_2]}{dt} = 0.028 [\text{Fe}^{3+}]. \quad (24)$$

It is difficult to render significance to the tenfold spread in the value of these first-order rate constants. However, experiment 4 with  $\text{FeCl}_3$  lixiviant has the highest overall rate constant. (None are really constant over time.) The rates expressed in this report are about 100 times slower than those reported by Singer and Stumm (13), but in reasonable agreement with the data of Boogard and others (17). Both these investigations involved shaker leaching experiments with small crystals of pyrite particles derived from coal, which tend to reduce or eliminate mass transport at the solid-liquid interface as a rate-controlling factor.

While a first-order rate process, as given above for the column leaching of pyrite from coal waste, can apparently be satisfied by the observed variation of rate of leaching with  $\text{Fe}^{3+}$  concentration, it cannot by itself account for the appearance of maxima in the concentration and rate data with time. This will require some appropriate time variation in the concentration of reactants and/or rate constant, as discussed in the next section.

## MECHANISMS

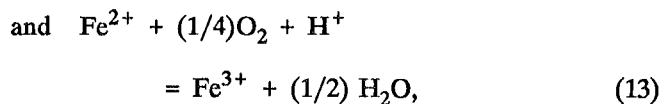
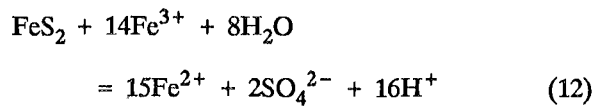
### Descriptive Considerations

The chemical mechanism of pyrite oxidation in an aqueous medium has been the subject of numerous studies (12), with the pyrite as purified crystals, in pyritic metal

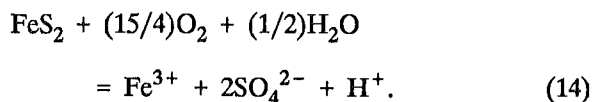
ores, or disseminated in a coal matrix. On a molecular level, there is still uncertainty about the elementary reaction steps involved in oxidative dissolution of the crystals of  $\text{FeS}_2$ . However, the overall mechanism as described by Singer and Stumm (13) is generally considered applicable to the pyrite leach process.

When pyrite particles are exposed to an aqueous medium containing  $\text{O}_2$  and  $\text{Fe}^{3+}$ ,  $\text{Fe}^{3+}$  is the dominant oxidant species as it adsorbs onto the surface of the pyrite particle and is reduced by the pyrite to the ferrous state. In the absence of  $\text{O}_2$ , the oxidation process becomes retarded by the preferential adsorption of the  $\text{Fe}^{2+}$  product onto the pyrite surface. However, in the presence of  $\text{O}_2$ , the adsorbed  $\text{Fe}^{2+}$  is oxidized to ferric, which then promulgates the pyrite oxidation reaction. In the course of the surface reactions, the sulfur in the pyrite is oxidized to elemental sulfur (without  $\text{O}_2$ ) or to  $\text{SO}_4^{2-}$  or some intermediate, such as thiosulfate (with  $\text{O}_2$ ). These surface processes, while not fully understood, are probably electrochemical in nature (19).

The cyclic process with  $\text{O}_2$  involves reactions given by equations 12, 13, and 14, as described previously and which are rewritten here:



with the net result being



Equation 13 is normally the slow step in establishing the rate of the net reaction in an acidic environment; however, it is readily catalyzed by bacteria normally present in acidic mine waters.<sup>15</sup> With bacterial catalysis of the reaction represented by equation 13, the slow step could revert to equation 12.

In the case of leaching pyrite from a coal matrix, the cyclic process represented by equations 12 and 13 can still occur, but it will require the transport of reactants and

<sup>14</sup>It is assumed in this study that during the first few days of leaching, the ferric ion content in the lixiviant would reflect the sulfate value of the starting coal waste. In the case of experiment 4, the starting lixiviant was a solution of  $\text{FeCl}_3$ .

<sup>15</sup>Singer and Stumm (13) report the half-life of the reaction given by equation 12 to be on the order of an hour, and the abiotic half-life of the reaction given by equation 13 to be about 1,000 days. Bacterial catalysis of the reaction given by equation 13 can increase its rate by more than a factor of 1 million.

products between the particle surface and the particle interior. The catalyzing bacteria [about 1  $\mu\text{m}$  in size (20)] are too large to enter the pores of the coal [0.02 to 0.2  $\mu\text{m}$  in size (21)], so they will tend to attach to the surface of the coal rather than to the actual pyrite surface. The reaction given by equation 13 with bacterial catalysis will then occur as  $\text{Fe}^{2+}$  is transported to the surface. Depending on the rates of diffusion of  $\text{Fe}^{2+}$  and  $\text{O}_2$  within the particle, equation 13 may occur in the particle interior without bacteria involvement even when bacteria are present at the surface of the coal.<sup>16</sup> The overall reaction, equation 14, being a coupling of chemical reaction and mass transport processes, will proceed at a rate corresponding to the slowest step in the coupled process, e.g., equation 12, equation 13, or intraparticle mass transport (i.e., diffusion of  $\text{O}_2$ ,  $\text{Fe}^{3+}$ , or  $\text{Fe}^{2+}$ ). Changing conditions, internal or external to the coal, initially or during the leaching process, can result in a change in the rate-controlling step. Such changes could readily account for apparent differences in results from different studies of pyrite leaching. They might also explain the appearance of a peak in the rate of reaction with time (figure 26). For example, decreasing coal particle size, and hence the time required for intraparticle diffusion, might change a diffusion-limited leach process to one that is chemically controlled and subject to bacterial catalysis. On the other hand, salt precipitation during leaching could increase the diffusion time, thereby causing the rate of reaction to decrease.

Previous investigators have concluded that the column leaching of pyrite from coal and rock is diffusion controlled (3). Strong evidence for this conclusion also comes from two findings in this current study:

1. The reaction rates determined for the four column experiments yield a half life ranging from 40 to 400 days, which is considerably longer than what would be expected if a bacterial catalyzed reaction, such as equation 13, was rate controlling.
2. The rate of desorption of THC is observed to correlate directly with both the rate of  $\text{O}_2$  consumption and the rate of sulfate production. Since THC desorption is prompted by processes that expand the coal matrix, such as heating (14) or  $\text{O}_2$  absorption, the rate of leaching is linked directly to the rates of desorption of THC and

<sup>16</sup>Cathles and Breen's (3) measurements of the diffusion of dilute KCl solutions in Illinois No. 6 and Wyoming coals indicate a value of about  $10^{-7} \text{ cm}^2/\text{s}$  for the diffusion coefficient. A 2-cm diffusion distance would take about 500 days, which is on the order of the abiotic reaction time for the reaction given by equation 13 (17).

absorption of  $\text{O}_2$  in the coal, i.e., a diffusion-controlled process.

### Model Considerations

The shrinking core model has general applicability to solids leaching processes and has been used to describe the leaching of pyrite from coal and rock (3, 22-23). The model considers a reaction front (or wave) starting at the surface of a coal particle and moving inward with a velocity that is controlled by the rate of transport of reacting species or their rate of chemical reaction. Ahead of the front is unreacted coal containing disseminated pyrite, and behind the front is reacted coal with pyrite leached out. Calculation of the velocity of the reaction wave can be quite complex when taking into account details of the rate(s) of various chemical reactions and the rate(s) of transport of various reactants and products through the reacted coal (23). When applying the model to an homogeneous, isotropic spherical particle, the rate of reaction,  $R_p$ , at time  $t$  can be expressed simply as

$$R_p(t) = 4\pi \rho_r [r - \lambda(t)]^2 v_r, \quad (25)$$

where  $r$  = particle radius,

$\lambda(t)$  = distance of reaction front from surface at time  $t$ ,

$v_r$  =  $d\lambda/dt$ , velocity of reaction front,

and  $\rho_r$  = density of solid reactant (pyrite) in coal.

It is easy to see that for a constant reaction front velocity,  $R_p$  always has its maximum when  $\lambda = 0$  or  $t = 0$ . The appearance of a reaction peak at some time other than zero would be indicative of a spatial heterogeneity in the material properties (e.g., reactant distribution and permeability) and/or a temporal change in the chemical rate constant (e.g., autocatalysis).

The A/D model of intraparticle diffusion was developed concurrently with the column leaching studies to treat the known spatial heterogeneity of porosity in coals (8). Using distribution theory to describe particle porosity, the model accounts for induction times and maxima in the rate of reaction directly in terms of the heterogeneous nature of the porosity. A recent modification to the A/D model also accounts for temporal changes in permeability, such as what could occur when leach product salts precipitate within the coal particle. For convenience, a brief description of the A/D model is given in appendix A. The basic rate equation for diffusion-limited reactions is a three-parameter expression (see appendix A),

$$R(t) = \frac{2he^{-\left[\ln\left(\frac{t+t_a}{t_b}\right)\right]^2}}{(t+t_a)\sqrt{\pi}(1-\text{erf}[\ln(t_a/t_o)])]}, \quad (26)$$

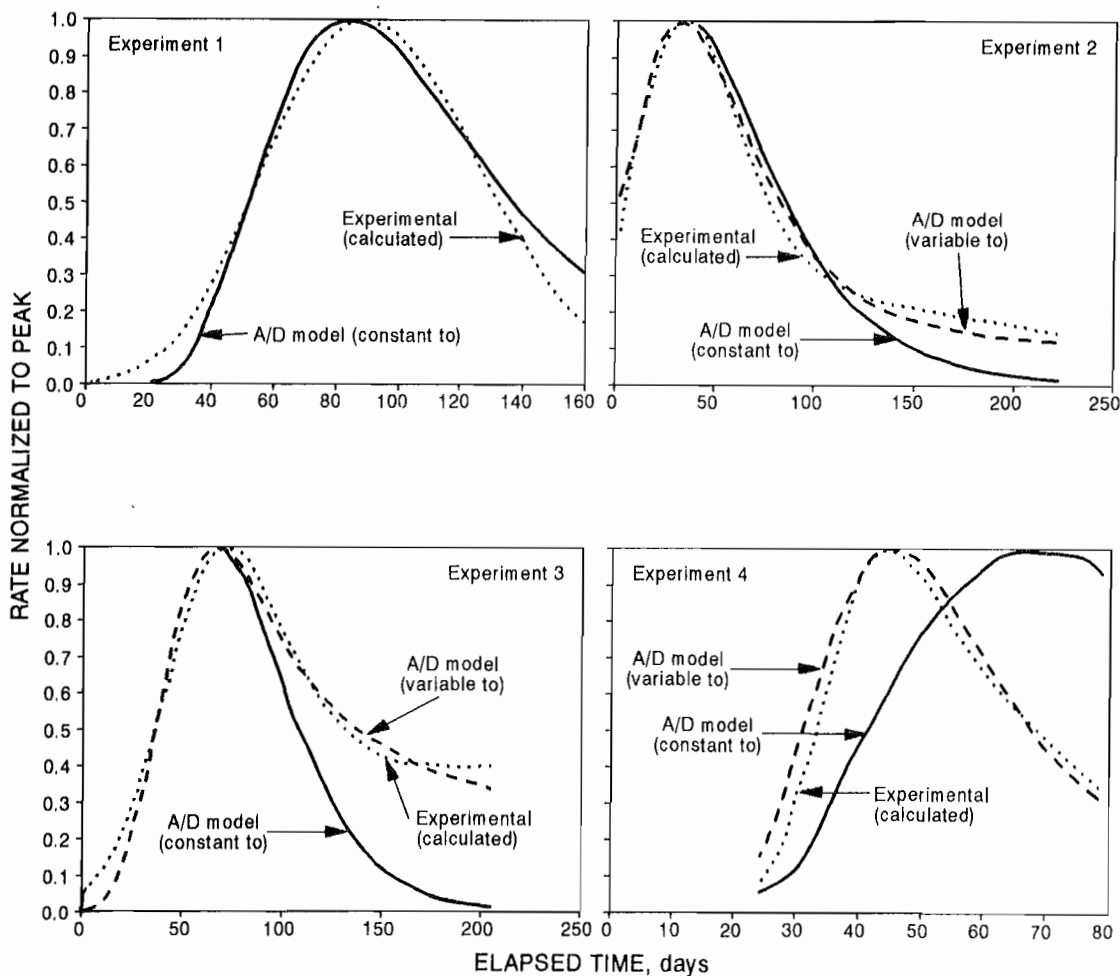
here,  $h$  and  $t_o$  relate to the distribution of material properties in an ensemble of coal particles and the mass transport coefficient; and  $t_a$  is a preaging time introduced to account for possible reaction prior to the start of an experiment (e.g., during storage). Time dependency in the particle permeability is achieved by allowing the parameter  $t_o$  to be some function of time, as expressed by the two-parameter equation

$$t_o(t) = t'_o(1 + je^{-k/t}). \quad (27)$$

Here,  $t'_o$  refers to the value of  $t_o$  at time zero and the parameters  $j$  and  $k$  can be chosen, *ad hoc*, to fit the rate data.

The ability of equations 26 and 27 to describe the pyrite leach rate data is demonstrated in figure 29, which compares the rates of pyrite reaction from experiments 1 to 4 (figure 26) with rates determined with a constant  $t_o$  and with a variable  $t_o$ . By normalizing the rate curves to their peak value, the comparison between the experimental and the A/D model rates can be visualized directly. The specific values employed for the various parameters are shown in table 7. As can be seen from the plotted curves, there is generally good agreement between the A/D model rates and the experimental (calculated) rates, particularly when a variable  $t_o$  is considered. While equations 26 and 27 are utilized here primarily as curve-fitting expressions, some

Figure 29



Comparison of A/D model rate of pyrite reaction calculations with experiment (calculated rates).

Table 7.—Experiments 1 to 4: A/D model curve-fit parameters

Parameter	Experiment 1		Experiment 2		Experiment 3		Experiment 4	
	Const <sup>1</sup>	Var <sup>2</sup>						
h . . . . .	1.7	NAp	1.7	1.7	2.5	2.5	1.7	1.7
t <sub>a</sub> , days . . . .	0	NAp	45	45	40	40	0	0
t <sub>0</sub> , days . . . .	100	NAp	95	95	115	115	80	80
c . . . . .	NAp	NAp	NAp	10	NAp	5	NAp	18
k . . . . .	NAp	NAp	NAp	200	NAp	400	NAp	200

Const Constant.

NAp Not applicable.

Var Variable.

<sup>1</sup>Refers to a constant t<sub>0</sub>.

<sup>2</sup>Refers to a variable t<sub>0</sub>.

attention is given to the fact that experiments 1, 2, and 4 involved the same basic coal waste. That is, the same value of the distribution property parameter, *h*, is maintained in each case. The range of values of *t*'<sub>0</sub> (i.e., 80 to 100 days) for the three coal waste experiments may or may not be significant in terms of suggesting differences in the diffusion process. However, comparing the values of *h* and *t*'<sub>0</sub> for coal waste with those for coal (experiment 3)

could suggest a narrower distribution of shortest distances (appendix A) and a longer mean diffusion time for the coal. The reaction rate for experiment 1 is described very well, with *t*<sub>0</sub> being constant over the entire elapsed time period. This suggests that, in this case, salt precipitates did not interfere with the intraparticle diffusion process—an interpretation that is consistent with the finding that about 80 pct of the pyrite was reacted.

## ACCELERATED LEACHING OF PYRITE

A practical objective of the trickle-bed column experiments was to examine how the leaching of pyrite in coal waste piles might be accelerated to reduce the long-term aspects of acid drainage from the waste piles. From the aspect of removing pyrite from coal waste, the use of FeCl<sub>3</sub> as a lixiviant (instead of water) led to a tenfold increase in the rate of pyrite removal by leaching. However, in terms of actually reducing the long-term pollution potential from the coal waste, this was not achieved. Even so, the mechanism study as it evolved in this work has led to a much better understanding of the constraints to accelerating the leach process and suggests a somewhat different approach to accelerating the acid drainage from coal waste heaps.

With coarse coal waste (2- to 4-cm particle size) typical of coal waste piles, it is probable that the rate of pyrite oxidation is diffusion limited by the transport of reactants (Fe<sup>3+</sup> and O<sub>2</sub>) in solution from the coal surface to the pyrite crystals, which are disseminated throughout the coal particle. The initial time constant for this diffusion-limited process is about 0.5 to 1.0 year, depending on the material properties (porosity) of the coal waste itself. However, as the oxidative solubilization of the pyrite progresses, salt precipitates (probably mixed iron hydroxy-sulfates, such as jarosite) form within the pores of the coal particle to slow down the diffusion process, possibly to the extent of nearly

stopping the pyrite oxidation. At this point, considerable pyrite is still available for reaction, but at a much slower rate, controlled now by leaching of the salt precipitates from the coal matrix. The coal pile will still be a significant source of acid drainage and pollution because of the continued leaching of the salt precipitates and the continued slow conversion of pyrite to salt precipitates. The time constant for this latter stage of leaching will be much greater than 1 year, so that the coal waste pile can be a source of pollution for many decades.

As described so far, the leaching process is not rate controlled by the presence of bacteria on the surface of the coal particle. This is because the abiotic chemical reactions involving oxidation of Fe<sup>2+</sup> to Fe<sup>3+</sup> by O<sub>2</sub> may still be faster than the diffusion of reactants through the coal matrix. If one speeds up the initial diffusion of reactants (e.g., by decreasing the size of the coal particles or increasing the mass transport coefficient), then chemical oxidation of Fe<sup>2+</sup> may become rate determining and bacteria at the coal surface will affect the overall rate of leaching. Alternatively, under conditions of very low-O<sub>2</sub> concentration, the abiotic rate of oxidation of Fe<sup>2+</sup> may become less than that of intraparticle diffusion, thus making the leaching process amenable to bacterial catalysis. This probably explains those reports where bacteria are noted to be important to the pyrite leaching process (11, 13)

and the effectiveness of detergent (bactericide) treatments in reducing acid drainage from coal waste piles (16). However, whether the leaching is abiotic or biotic, salt precipitates will probably still build up with time, so that leaching will eventually revert to an even slower process of

solubilization of salt precipitates. Thus, from an accelerated leaching point of view, it would be desirable to develop lixiviant conditions (acid base or biomediated) that will prevent salt precipitates from forming and/or cause them to become more readily solubilized.

## CONCLUSIONS

This report concludes column reactor studies specifically designed to improve our understanding of the coupling of chemical reaction and mass transport as rate processes that occur during the leaching of solids. In particular, it was hoped to develop and demonstrate a diagnostic methodology by which these rate processes can be elucidated and measured while they are experimentally coupled, rather than in the more conventional approach of investigating their rates separately in an uncoupled mode. This was achieved utilizing data from an experimental study of the leaching of pyritic coal waste in a counterflow, trickle-bed column reactor. In spite of numerous problems with lixiviant and solid sampling within the column, adequate data were obtained to demonstrate that:

1. The counterflow, trickle-bed, packed-column reactor yields pertinent information relating chemical and transport phenomenon as they are actually coupled in a solids leaching process;
2. The diagnostic methodology can be applied to column leaching data such that pertinent chemical reactions and transport processes, and overall mechanisms are elucidated as they are actually coupled, and;

3. Achieving the removal of sulfate from coal and coal waste by leaching requires methods to prevent iron salts (perhaps as jarosites) from precipitating within the coal particles.

The A/D model of solids leaching, which was developed as an outcome of the experimental studies, represents a significant adjunct to the diagnostic methodology and offers an approach to accounting for heterogeneity (e.g., size, shape, permeability, and chemical composition and distribution) in multiphase solids reaction processes. In this current leaching study, consideration of a lognormal distribution for the intraparticle permeation distance, combined with the assumption of a diffusion-limited leaching process, yields a generic rate equation that can describe the observed rates of leaching of pyrite from coal. With appropriate leach data and analyses, it might eventually be possible to convert the A/D model from a descriptive model (i.e., with curve-fit parameters) to a predictive model (i.e., with predetermined parameters). This latter development will be the key to demonstrating the utility of the A/D model (or any other model) of solids leaching.

## ACKNOWLEDGMENTS

The authors recognize the following individuals for their contributions during the course of this work: C. R. Manns, physical science technician, Pittsburgh Research Center's (PRC's) Environmental Technology Group, who assisted in the execution of the column leach experiments, which gave rise to the data without which this work would not have been possible; and D. H. Finseth, supervisory

physical scientist, U.S. Department of Energy's Pittsburgh Energy Technology Center; H. M. Edenborn, supervisory research biologist; R. W. Hammack, geologist; A. G. Kim, supervisory physical scientist; and R. L. P. Kleinmann, research supervisor, PRC's Environmental Technology Group, who by numerous discussions helped lead the way to ideas to pursue.

## REFERENCES

1. U.S. Bureau of Mines. In Situ Leach Mining. USBM IC 9216, 1989, 107 pp.
2. Cathles, L. M., and J. A. Apps. A Model of the Dump Leaching Process That Incorporates Oxygen Balance, Heat Balance and Air Convection. *Metall. Trans.*, v. 6B, 1975, pp. 617-624.
3. Sareen, S. S., R. A. Giberti, P. F. Irminger, and L. T. Petrovic. The Use of Oxygen/Water for Removal of Sulfur From Coals. *AIChE Symp. Ser.* 73, No. 165, 1977, pp. 183-189.
4. Jackson, D. R., and D. L. Bisson. Comparison of Laboratory Batch Methods and Large Column for Evaluating Leachate From Mono-filled Solid Wastes. *J. Air Waste Manage. Assoc.*, v. 40, 1990, pp. 1514-1521.
5. Jeffers, T. H., C. R. Ferguson, and P. G. Bennett. Biosorption of Metal Contaminants Using Immobilized Biomass—A Laboratory Study. USBM RI 9340, 1991, 9 pp.
6. Doyle, F. M., and A. H. Mizza. Understanding the Mechanisms and Kinetics of Acid and Heavy Metal Release From Pyritic Wastes. Paper in Proceedings of the Western Regional Symposium on Mining and Mineral Processing of Wastes, ed. by F. M. Doyle. *Soc. Min. Eng.*, Littleton, CO, 1990, pp. 43-51.
7. Dalverny, L. E., and R. F. Chaiken. Leaching of Pyrite From Coal Wastes in a Trickle-Bed Reactor. *Environmental Issues and Waste Management in Energy and Minerals Production*, ed. by R. K. Singhal, A. K. Mehrotra, K. Fytas, and J. Collins. Balkema, Rotterdam, Netherlands, 1992, pp. 435-445.
8. Chaiken, R. F. An Absorption/Desorption Model of Solids Leaching. *Geochim. Cosmochim. Acta*, v. 56, 1992, pp. 2589-2593.
9. Fredrickson, A. G., and R. B. Byrd. Transport Phenomena in Multicomponent Systems. Ch. 6 in *Handbook of Fluid Dynamics*, ed. by V. L. Streeter. McGraw-Hill, New York, 1961, pp. 6-1 to 6-56.
10. Sharp, F. A. Biologically Mediated Depyritization of Large Sized Coal. Paper in the Ninth Annual International Pittsburgh Coal Conference. Univ. Pittsburgh, Pittsburgh, PA, 1992, pp. 95-100.
11. Hammack, R. W., D. M. Hyman, G. J. Olson, D. H. Finseth, and K. H. Rhee. Microbial Depyritization of a Problematic High Sulfur Coal. Paper in Proceedings: 1991 Second International Symposium on the Biological Processing of Coal. *Electr. Power Res. Inst.*, Palo Alto, CA, 1991, pp. 3-15 to 3-34.
12. Lawson, R. T. Aqueous Oxidation of Pyrite by Molecular Oxygen. *Chem. Rev.*, v. 82, 1982, pp. 461-497.
13. Singer, P. C., and W. Stumm. Acid Mine Drainage: The Rate-Determining Step. *Science*, v. 167, 1970, pp. 1121-1123.
14. Kim, A. G. Laboratory Determination of Signature Criteria for Locating and Monitoring Abandoned Mine Fires. USBM RI 9348, 1991, 19 pp.
15. Deul, M., and E. A. Mihok. Mine Water Research. Neutralization. USBM RI 6987, 1967, 24 pp.
16. Kleinmann, R. L. P., and P. M. Erickson. Control of Acid Drainage From Coal Refuse Using Anionic Surfactants. USBM RI 8847, 1983, 16 pp.
17. Boogard, F. C., C. van den Beemd, T. Stoelwinder, P. Bos, and J. G. Kuenen. *Biotechnol. and Bioeng.*, v. 38, 1991, pp. 109-115.
18. U.S. Bureau of Mines. Methods of Analyzing and Testing Coal and Coke. *Bull.* 638, 1967, pp. 11-12.
19. Moses, C. O., and J. S. Herman. Pyrite Oxidation at Circum-neutral pH. *Geochim. Cosmochim. Acta*, v. 55, 1991, pp. 471-482.
20. Ehrlich, H. L. *Geomicrobiology*. Marcel Dekker, New York, 2nd ed., 1990, p. 291.
21. Sharkey, A. G., Jr., and J. T. McCartney. Physical Properties of Coal and Its Products. Ch. in *Chemistry of Coal Utilization*, ed. by M. A. Elliott. Wiley, 2nd suppl. v., 1981, pp. 159-283.
22. Pantelis, G., and A. I. M. Ritchie. Macroscopic Transport Mechanisms as a Rate-Limiting Factor in Dump Leaching of Pyrite Ores. *Appl. Math. Model.*, v. 15, 1991, pp. 136-143.
23. Batarsch, K., G. P. Swaney, and A. H. Stiller. A Mathematical Model for Heterogeneous Reactions With a Moving Boundary. *AIChE J.*, v. 35, 1989, pp. 625-634.

## APPENDIX A.—A/D MODEL OF SOLIDS LEACHING

The A/D model of solids leaching (8) is similar to the shrinking core model for a diffusion-limited rate process in that it assumes the reaction front moves by diffusive flow within the particle. In the A/D model, heterogeneity in mass transport is accounted for directly by considering the particle to be composed of regions of microporosity and macroporosity, the latter defined by cracks, channels, and the particle surface itself. The reaction front is then considered to be one dimensional in the sense that it moves along paths of "shortest distance" between points within the micropore region and points of the macropore region (figure A-1). Diffusion from the particle surface (i.e., absorption) or diffusion to the particle surface (i.e., desorption) is determined only by the flow in the micropore region—the flow in the micropore region being much slower than the flow in the macropore region. It is assumed that the number of paths of shortest distance,  $\lambda$ , for a single particle or for an ensemble of particles, can be described by a normalized frequency distribution,  $f(\lambda)$ , so that

$$dn(\lambda) = f(\lambda)d\lambda \quad (\text{A-1})$$

defines the fraction,  $dn(\lambda)$ , of shortest distance paths lying between  $\lambda$  and  $\lambda + d\lambda$ . Diffusion is a wave front that moves with velocity  $v_\mu = d\lambda/dt$  along each shortest distance path (figure A-2). The time rate of consumption of paths is the overall rate of diffusion, which for a diffusion-controlled reaction defines the rate of reaction  $R_p$ . That is, the extent of reaction after a given length of time is

$$R_p = dn(\lambda)/dt = f(\lambda)v_\mu, \quad (\text{A-2})$$

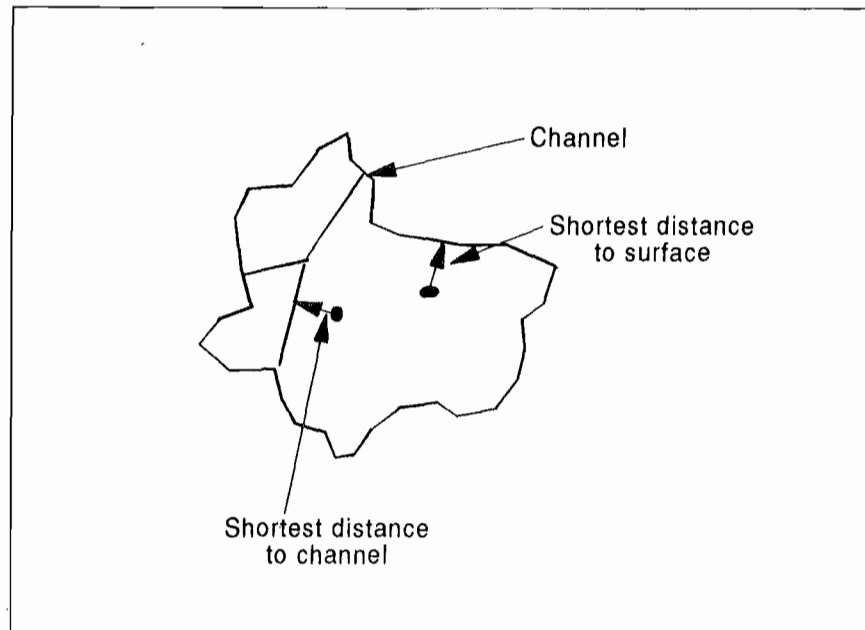
and

$$P(t) = \int_0^t f(\lambda)v_\mu dt. \quad (\text{A-3})$$

These equations (A-2 and A-3) assume that all reaction starts at  $t = 0$ , defined at the start of some experiment. If the reaction actually starts at a time,  $t_a$ , before the experiment (e.g., preaging), but the start of the experiment still defines  $t = 0$ , the rate equation appropriate to defining the experimental data will be modified, i.e.,

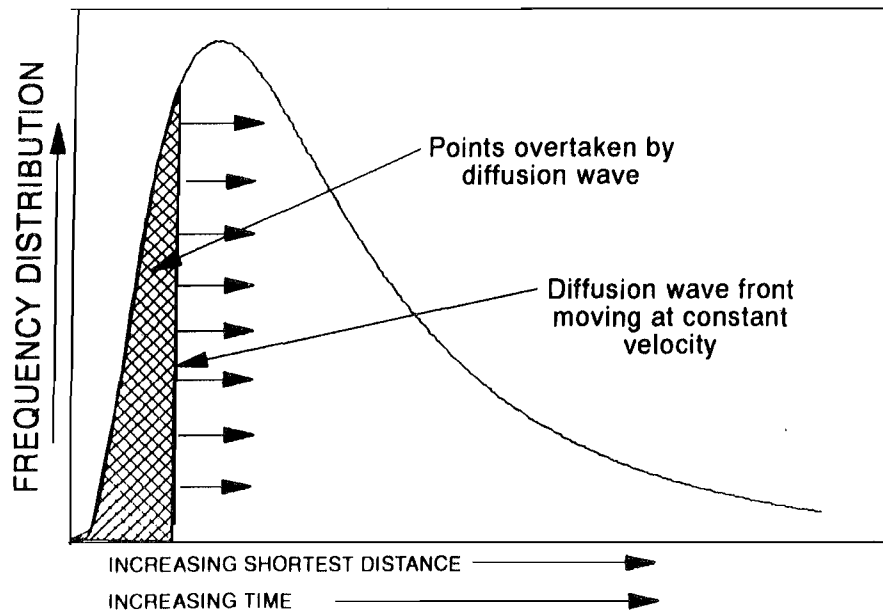
$$R(t) = \frac{R_p(t + t_a)}{1 - P(t_a)}. \quad (\text{A-4})$$

*Figure A-1*



*Examples of shortest distances in particle.*

Figure A-2



Representation of diffusion process in A/D model.

The denominator in equation A-4 simply renormalizes the fractional extent of reaction to account for any change in the initial amount that can react.

Assuming a lognormal distribution for  $f(\lambda)$ , i. e.,

$$f(\lambda) = \frac{h}{\lambda\sqrt{\pi}} e^{-h^2[\ln(\lambda/\lambda_0)]^2}, \quad (\text{A-5})$$

where  $h$  = spread factor of distribution (related to variance)

and  $\lambda_0$  = mean of distribution.

A three-parameter expression for the rate of reaction is obtained, i.e.,

$$R(t) = \frac{2he^{-\left[h\ln\left(\frac{t+t_b}{t_0}\right)\right]^2}}{(t+t_a)\sqrt{\pi}\left(1-\text{erf}\left[h\ln\left(\frac{t+t_b}{t_0}\right)\right]\right)}. \quad (\text{A-6})$$

The parameters are  $t_0 = \lambda_0/v_\mu$ , which is the time for the diffusion front to travel the mean shortest distance; the preaging time,  $t_a$ ; and  $h$ , the spread of the distribution function. Equation A-6 is the same equation derived originally and used with success to curve fit data for a number of different solids leaching experiments.<sup>1</sup>

<sup>1</sup>The equation as it appears in reference 8 contains a typographical error.

Since the original development of the A/D model (8), equation A-6 was modified to account for the effect of salt precipitation in the solid phase on the rate of reaction. This was accomplished by recognizing that such salt precipitation would tend to alter the permeability of the solid phase, i.e., to decrease the diffusion velocity,  $v_\mu$ , during the course of leaching. This effect is simulated in the A/D model by introducing, *ad hoc*, a time dependency in  $t_0$ . A time-dependent function,  $t_0(t)$ , was chosen with the following attributes: (1) being continuous and single valued over all time, (2) having a finite value at time zero, and (3) increasing at some point in time to a limiting value. These attributes are achieved by the two-parameter function:

$$t_0(t) = t'_0(1 + je^{-k/t}). \quad (\text{A-7})$$

With an appropriate value for  $k$ , the exponential term can emulate almost any decreasing function in time, including a step function.

Figure 29 shows the ability of equations A-6 and A-7 to curve fit the rate of leaching of pyrite as determined by the trickle-bed column experiments. In this figure, both the experimental data and the A/D model calculations have been normalized to their respective value at the peak of reaction, which automatically accounts for the numerical factor used in correcting for the appearance of excess sulfur in the solids analysis. The agreement between the data and equation A-6, which is quite good at constant  $t_0$  for experiments 1 to 4, becomes even better by considering  $t_0(t)$ .

## APPENDIX B.—LIST OF SYMBOLS

$a, b, c, p$	stoichiometric coefficients for $\alpha, \beta, \gamma,$ and $P,$ respectively
$a', b', c'$	kinetic reaction orders for $\alpha, \beta,$ and $\gamma,$ respectively
$f, F, g, G$	various concentration functions of time and distance
$k_r$	kinetic rate constant
$n(\lambda)$	fraction of points having shortest distance, $\lambda$ (in A/D model)
$P$	product of reaction
$r$	particle radius
$R_p$	kinetic rate of formation of $P$ in column
$R_{\alpha, \beta, \gamma}$	kinetic rate of reaction of reactant components in column
$s$	saturation (ratio of liquid to void volume)
THC	total C1 to C5 hydrocarbon gases (methane, ethane, propane, butane, and pentane)
$t', j, k$	parameters of A/D model relating to change of $t_0$ with time
$v_r$	reaction front velocity in shrinking core model of leaching
$v_{\alpha}, v_{\beta}$	effective linear flow velocity of gas and liquid phases, respectively (ratio of volumetric flow rate to cross-sectional area of column reactor)
$v_{\mu}$	velocity of diffusion wave front (in A/D model)
$\alpha, \beta, \gamma$	reactants of gas, liquid, and solid phases, respectively; also concentration of component of that phase
$\epsilon$	porosity (ratio of void to bulk volume)
$\lambda, h, t_a$	parameters of A/D model
$\rho_r$	density of solid reactant (pyrite) in coal particle
$\phi, \psi, \theta$	concentration of reactants in gas, liquid, and solid phases, respectively (functions of $t$ and $x$ )
$(\phi)_t, (\phi)_x$	partial derivatives with respect to $t$ and $x,$ respectively